Temperature variations during the past 20 ka at Huguangyan Maar Lake in tropical China and dynamic link

Qi Li[1], Qing Sun[2], Manman xie[3], Yuan Ling[4], Zeyang Zhu[5], Qingzeng Zhu[3], Nan Zhan[2], and Guoqiang Chu[3]

[1]Institute of Geology and Geophysics
[2]National Research Center of Geoanalysis
[3]Key Laboratory of Cenozoic Geology and Environment, Institute of Geology and Geophysics, Chinese Academy of Sciences
[4]Institute of Mineral Resources, Chinese Academy of Geological Sciences
[5]Institute of Geology and Geophysics Chinese Academy of Sciences

November 23, 2022

Abstract

Discrepancies exist in global temperature evolution from the Last Glacial Maximum to the present between model simulations and proxy reconstruction. This debate is critical for understanding and evaluating current global warming on a longer timescale. Here we report a branched GDGTs-based temperature reconstruction from the sediments of Huguangyan Maar Lake in southeast China and validate it using historical documentary evidence and instrumental data. The reconstructed mean annual air temperature (MAAT) indicates distinct changes during the last deglaciation (Oldest Dryas, Bølling-Allerød, Younger Dryas). During the Holocene, temperatures gradually increased from the end of the Younger Dryas to ˜7.0 ka BP, followed by a decrease in recent decades. However, our terrestrial temperature record differs from model simulations and proxy sea surface temperature records of the Holocene. We conclude that ice volume or ice sheet is the most prominent forcing that controlled the regional temperature evolution from the Last Glacial Maximum to the beginning of the middle Holocene; while the temperature variations during the middle and late Holocene were mainly regulated by several possible factors, such as oceanic and atmospheric circulation, and external drivers (solar and volcanic activity).

Temperature variations during the past 20 ka at Huguangyan Maar Lake in tropical China and dynamic link

Qi Li[1,2], Qing Sun[3], Manman Xie[3], Yuan Ling[4], Zeyang Zhu[1], Qingzeng Zhu[1], Nan Zhan[3], Guoqiang Chu[1,5,6]

[1]Institute of Geology and Geophysics, Chinese Academy of Sciences, Beijing 100029, China.

[2] University of Chinese Academy of Sciences, Beijing 100049, China.

[3] National Research Center of Geoanalysis, Beijing 100037, China.

[4] Institute of Geology, Chinese Academy of Geological Sciences, Beijing 100037, China.

[5] CAS Center for Excellence in Life and Paleoenvironment, Beijing 100044, China.

[6] Innovation Academy for Earth Science, Chinese Academy of Sciences, Beijing 100029, China.

Corresponding author:

G. Chu (chuguoqiang@mail.igcas.ac.cn) and Q. Sun (sunqing1616@yahoo.com)

Key Points:

- A temperature record over last 20 ka from Huguangyan Maar Lake in tropical China based on brGDGTs
- The Holocene temperature evolution at Huguangyan Maar Lake characterized with a regional-scale temperature change
- Ice volume may be main driving force on the temperature change of Huguangyan Maar Lake region from the Last Glacial Maximum to Holocene

Abstract

Discrepancies exist in global temperature evolution from the Last Glacial Maximum to the present between model simulations and proxy reconstruction. This debate is critical for understanding and evaluating current global warming on a longer timescale. Here we report a branched GDGTs-based temperature reconstruction from the sediments of Huguangyan Maar Lake in southeast China and validate it using historical documentary evidence and instrumental data. The reconstructed mean annual air temperature (MAAT) indicates distinct changes during the last deglaciation (Oldest Dryas, Bølling-Allerød, Younger Dryas). During the Holocene, temperatures gradually increased from the end of the Younger Dryas to ˜7.0 ka BP, followed by a decrease in recent decades. However, our terrestrial temperature record differs with model simulations and proxy sea surface temperature records of the Holocene. We conclude that ice volume or ice sheet is the most prominent forcing that controlled the regional temperature evolution from the Last Glacial Maximum to the beginning of the middle Holocene; while the temperature variations during the middle and late Holocene were mainly regulated by several possible factors, such as oceanic and atmospheric circulation, and external drivers (solar and volcanic activity).

1 Introduction

There is an ongoing debate about the Holocene temperature record of the extratropical Northern Hemisphere. Proxy records show a general long-term cooling trend since the early Holocene (Marcott et al., 2013), while model simulations indicate a warming trend over the past ˜12,000 years (Liu et al., 2014). Models play an important role in understanding how climate systems respond to various forcing factors and boundary conditions. However, many dynamic processes are not well computed or weighted in the model simulations, such as external forcing factors (solar irradiance and explosive volcanism), and the internal variability of the climate system (e.g., ENSO, PDO, AO, and the monsoon). Moreover, proxy-based temperature reconstructions are often of low resolution and have relatively large uncertainties in proxy calibration and dating, as well as regional or seasonal biases. Hence, more regional proxy-based paleoclimate time series are needed to verify the climatic record of the Holocene and to understand the differences between model simulations and paleoclimate reconstructions.

In this study, we present a high resolution branched glycerol dialkyl glycerol tetraethers (brGDGTs) membrane lipids-based temperature reconstruction (0-10 ka BP) combined with previously published data (10-20 ka BP) from the sediments of Huguangyan Maar Lake (21º9'N, 110º17'E) in tropical China (Chu et al., 2017), with the aim of obtaining a regional terrestrial temperature record and to understand its dynamic links.

Our paleotemperature proxy is based on brGDGTs, which comprise two dialkyl chains with different amounts of methyl and cyclopentane moieties (Damsté et al., 2009; Hopmans et al., 2004; Naafs et al., 2017; Sanchi et al., 2014; Schouten et al., 2000; Schouten et al., 2013; Sun et al., 2011; Tierney & Russell, 2009; Weijers et al., 2007). The physical and biological mechanisms of the temperature sensitivity of brGDGTs could be due to their membrane components maintaining membrane fluidity via methyl and cyclopentane moieties (Damsté et al., 2002; Huguet et al., 2007; Weijers et al., 2007). The methylation index of branched tetraethers (MBT) and the cyclization ratio of branched tetraethers (CBT) have previously been used to reconstruct terrestrial paleotemperatures from lacustrine sediments, soils, and peat sequences (Ding et al., 2015; Naafs et al., 2017; Peterse et al., 2012; Weijers et al., 2007; Yang et al., 2014).

Numerous studies have confirmed that brGDGTs-based indices from lacustrine sediments can be used to reconstruct terrestrial paleotemperatures (De Jonge et al., 2014; Hu et al., 2016; Kaiser et al., 2015; Loomis et al., 2012; Martin et al., 2020; Naafs et al., 2017; Pearson et al., 2011; Russell et al., 2018; Sun et al., 2011;

Tian et al., 2019; Tierney et al., 2010; Weijers et al., 2007; Zink et al., 2016). However, several interpretational uncertainties remain, such as regarding the relative contributions of aquatic sources and soil sources to brGDGTs because the calibration functions from soils and lakes are quite different. Huguangyan Lake is a small, hydrologically-closed lake with no inflows and a small watershed area, and therefore the sedimentary organic matter originates mainly in the water column (Chu et al., 2017; Hu et al., 2016). The within-lake origin of the sedimentary organic matter, which is also supported by the relatively low sedimentary TOC/N ratios since ~20 ka BP (Chu et al., 2002), substantially reduces this source of uncertainty in paleotemperature reconstruction. Previous brGDGTs-based MAAT reconstructions during the last deglaciation from the sediments of Huguangyan Maar Lake demonstrated a distinctive pattern of temperature changes from during the Oldest Dryas, Bølling-Allerød, Younger Dryas, and the onset of the Holocene (Chu et al., 2017).

2 Materials and Methods

2.1 Study site

Maar lakes are recognized as ideal sites for preserving high-resolution sedimentary archives because they are closed basins with a relatively simple hydrological system and they provide continuous sedimentary sequences (Yancheva et al., 2007). Huguangyan Maar Lake is a closed basin without stream inputs located in the Leizhou Peninsula in the tropical region of South China. The surface area is 2.3 km2, the maximum water depth is 22 m, and the watershed area is 3.2 km2 (Figure 1) (Chu et al., 2002; Yancheva et al., 2007). The area has a mean annual air temperature of 23.4 and a temperature difference between winter and summer of 11.9 (1964–2004; data from Zhanjiang meteorological station). Overlapping piston cores were collected from near the center of the lake in a water depth of 14 m. The cores were sliced at a 1-cm interval and then freeze dried for GDGTs extraction.

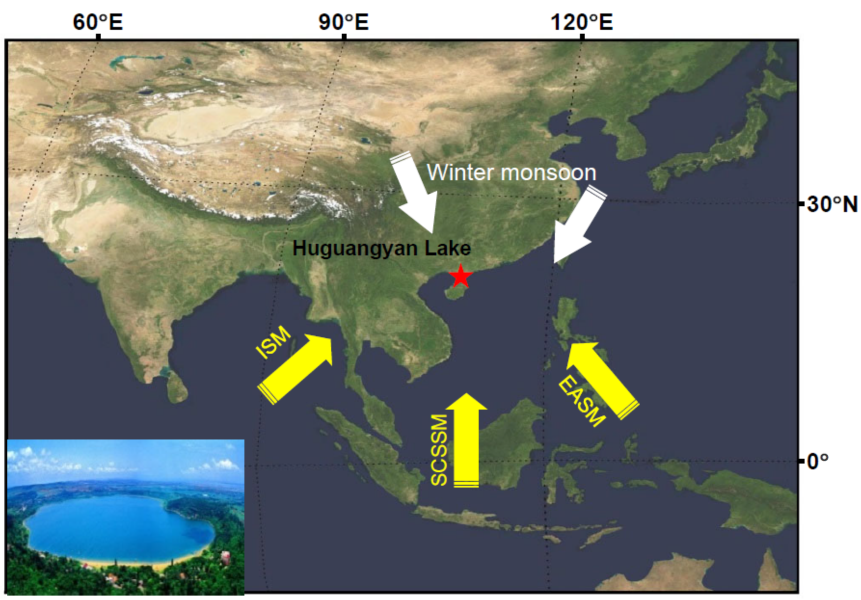

Figure 1. Location of Huguangyan Maar Lake. Solid arrows indicate the dominant direction of the summer monsoon (yellow) and winter monsoon (white). The inset photo shows Huguangyan Lake. Background image is modified from NASA (*http://visibleearth.nasa.gov*).

2.2 Chronology

The sedimentary chronology for Huguangyan Maar Lake is based on 14 AMS^{14}C dates from handpicked leaves and/or other terrestrial plant macrofossils, together with analyses of^{137}Cs and ^{210}Pb concentrations

(Table 1; Figure 2; Supplementary Figure S1). The results of radiometric dating (^{137}Cs, ^{210}Pb, AMS^{14}C) have been presented previously (Chu et al., 2017; Wang et al., 2016).

Table 1. Radiocarbon ages from Huguangyan Maar Lake.

Lab. code	**Material**	**Depth (cm)**	**Radiocarbon age (BP)**	**Calibrated age (Median)**
Poz-47119	Leaves	53	850±40	738
Poz-47120	Leaves	94	1200±50	1135
Poz-47121	Branch	135	1275±30	1233
Poz-47122	Leaves	179	1875±35	1822
Poz-47187	Leaves	290	3650±35	3941
Poz-47123	Leaves	399	4140±40	4644
Poz-47124	Leaves	541	6280±40	7215
Poz-47188	Leaves	626	9420±80	10640
Poz-47125	Leaves	671	10300±70	12246
Poz-47127	Leaves	731	11430±60	13427
Poz-47128	Leaves	815	13420±70	16122
Poz-47129	Charcoal	882	14530±170	17399
Poz-47130	Charcoal	936	15590±120	18619
Poz-47131	Charcoal	1026	16980±200	20219

All AMS ^{14}C ages were calibrated using the atmospheric data set from the calibration program CALIB 4.3 (Stuiver et al., 1998).

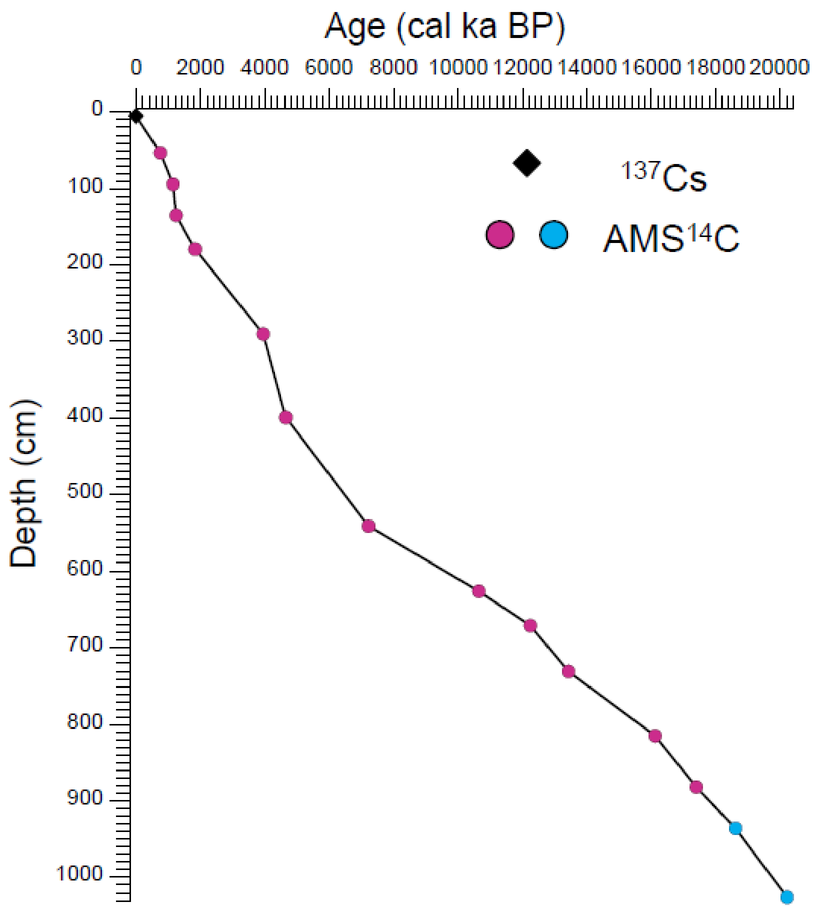

Figure 2. Age-depth plot for the Maar Lake Huguangyan. The calibrated AMS14C dates are from Wang et al., (2016) (red) and Chu et al., (2017) (blue).

2.3 GDGTs analysis

This study builds upon previous work of Huguangyan Maar Lake (Chu et al., 2017). For GDGTs analysis, freeze-dried samples (˜1.5 g) were extracted using a dichloromethane (DCM): methanol (9:1, v/v) mixture with an accelerated solvent extractor (ASE 350) at 120 and 1500 psi for two cycles. The extracts were dried under N_2 and separated into apolar and polar fractions over an activated Al2O3 column using hexane: DCM (9:1, v/v) and DCM: methanol (1:1, v/v) as the respective eluents.

The branched GDGTs were analyzed using a Shimadzu high-performance liquid chromatography triple quadrupole mass spectrometry system (HPLC-MS), with an autosampler and Analyst software (modified by Hopmans et al., 2004; Weijers et al., 2007). Separation was achieved using a Grace Prevail Cyano column (150 mm × 2.1 mm; 3 µm); ion scanning was performed in a single ion monitoring mode at m/z 1050, 1048, 1046, 1036, 1034, 1032, 1022, 1020 and 1018. The brGDGTs were quantified using a C46 internal standard.

MAAT from brGDGT for the Huguangyan Maar Lake was obtained using the degree of methylation (MBT) and the cyclisation ration of branched tetraether (CBT) according to the proxy calibration for the lacustrine sediment from China and Nepal (Sun et al., 2011):

$$MAAT=3.949 - 5.593 \times CBT + 38.213 \times MBT \quad (n=100,\ r^2=0.73)$$

3 Result and Discussion

3.1 Reconstruction temperature vs. instrumental data and historical documentary.

All proxy data are indirect measurements of climate change, and therefore it is necessary to calibrate or validate them against instrumental or other independent data(Jones & Mann, 2004). Hence, we compared the brGDGTs-based MAAT record from Huguangyan Maar Lake with several other independent climate datasets: instrumental annual mean air temperature data from Zhanjiang meteorological station, ˜15 km from Huguangyan Lake; historical documents from 140 local chronicles and 14 monographs from southern China (south of 23.5^{o}N), and a synthetic temperature reconstruction for China (Figure 3c).

The reconstructed MAAT is 22.5 for the period of 2010 CE–1951 CE (based on 137Cs-dating of the uppermost part of the sediment column). This result is close to the instrumental annual mean air temperature (23.2) for the same period obtained from nearby Zhanjiang meteorological station, however, there is a 0.7 offset between the instrumental data and the reconstructed temperatures. Although temperatures in this tropical lake are favorable for biological activity throughout the year, the brGDGTs-based temperature is slightly biased to winter and spring temperatures because of the turnover of the water column, which causes nutrient-rich bottom water to reach the surface and support the growth of aquatic organisms. This was confirmed by the seasonal flux of brGDGTs estimated from sediment traps (Hu et al., 2016), together with monthly observations of planktonic diatoms (Wang et al., 2012). The occurrence of lower temperatures during the 1970s is confirmed by both instrumental data for 1921 CE–1939 CE and 1951 CE–2010 CE, as well as by the MAAT reconstruction (Figure 3a).

Historical documents have often been used for paleoclimatic reconstruction. In tropical China, historical documents are widely available and there are hundreds of local chronicles. Direct descriptions using terms such as “rivers frozen” and “snow, sleet and frost” in tropical China (south of 23o30’ N) are interpreted as clear evidence of cold events. These abnormal phenomena are related to cold surges (cold waves). Meteorologically, a cold surge has been defined as a very large temperature decrease (exceeding 8) within 24 hours, and they are proposed as a surrogate for winter monsoon strength in China (Ray et al., 1991). Cold surges have a relatively short duration, often less than one week. We used historical documents to produce a compilation of evidence of “rivers frozen, snow, sleet and frost in the tropical plains” (south of 23.5o N; see Supplementary Table S1). The sources are from ”Natural disasters in historical documents in Guangdong province” (including Hainan province) and ”Natural disasters in historical documents in Guangxi province” (Institute of Literary and History, Guangdong Province, unpublished data), which consist of 140 local chronicles and 14 monographs.

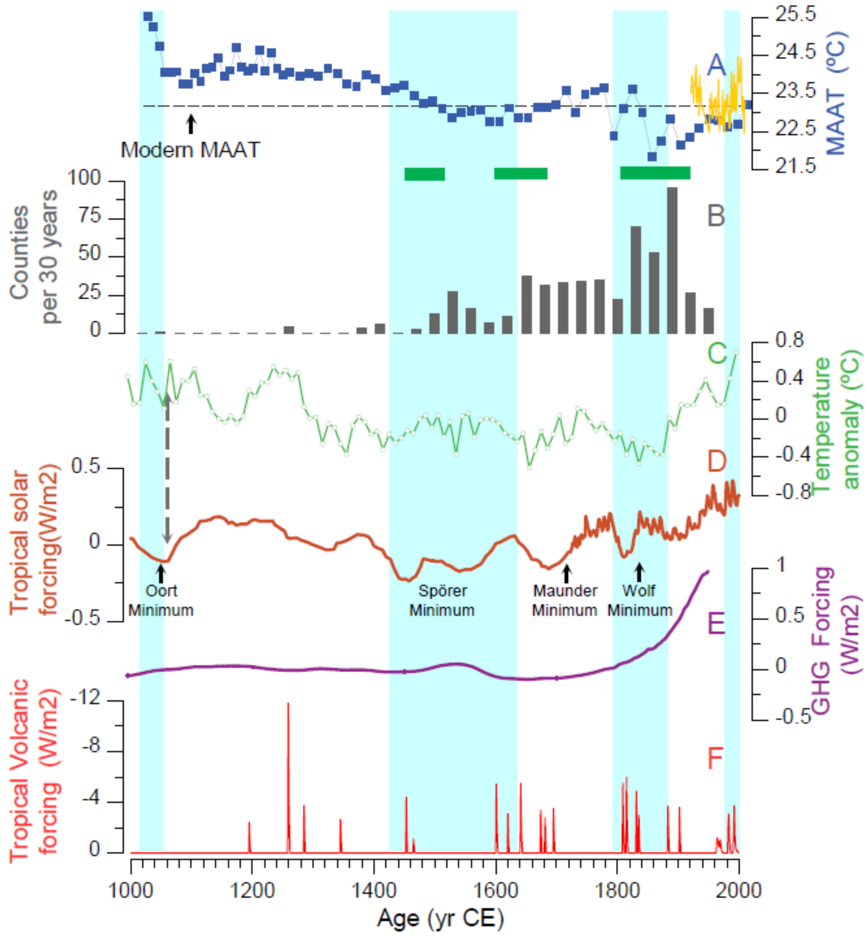

Figure 3. Comparison of the brGDGTs-based MAAT record for Huguangyan Maar Lake with historical documentary evidence, instrumental data, and possible climate forcings during the last millennium. (**a**) brGDGTs-based MAAT record obtained in this study (blue line); annual mean air temperature from Zhangjiang Station (1921–1939 and 1951–2010) (yellow line); modern MAAT for the study area (green dashed line). (**b**) Number of counties with cold surges per 30 years in tropical China years from historical documents; (**c**) Synthetic temperature reconstruction for China (Ge et al., 2015); (**d**) Record of tropical solar forcing (Mann et al., 2005); (**e**) record of GHG radiative forcing (CO_2, CH_4, N_2O) (Köhler et al., 2017); (**f**) Record of tropical volcanic forcing (Mann et al., 2005); Green bars represent the extreme cold winters based on historical documentary evidence from China (Chu and Ching, 1973).

Extreme cold events are concentrated in the Little Ice Age, especially between 800 CE and 1900 CE, while the Medieval Warm Period (MWP) had few fewer cold events (Figure 3b). Historical records are less abundant and intermittent before 1400 CE but are more continuous after the Ming Dynasty (the Fang Zhi (local chronic) period of 1400 CE-1900 CE). The brGDGTs-based MAAT record from Huguangyan Maar Lake shows three cold intervals: 440 CE-1640 CE, 1800 CE-1890 CE, and during the 1970s (Figure 3a). Within the limits of the dating uncertainties, these intervals are consistent with the documentary evidence (Figure 3b).

Natural climate forcings such as changes in solar output and volcanic eruptions are widely recognized as causes of decadal-to-centennial–scale climatic variations. Figure 3 shows that most of the cold intervals recorded at Huguangyan Maar Lake correspond to sunspot minima and episodes of intensified volcanic activity. However, the decrease in MAAT at ~1740 CE is not linked to these forcings.

3.2 Holocene brGDGTs-based temperature change

Although the climate of the Holocene, the most recent interval of Earth history, was more stable than that during the last glacial period, it was interrupted by several abrupt cooling events on the decadal- to centennial-scale (Bond et al., 2001). The brGDGTs-based temperature record from Huguangyan Maar Lake shows an increase in MAAT from 22 after the Younger Dryas (11.5 ka BP) to 28 by ~7.0 ka BP, followed by a gradual decrease from 23.5 in recent decades. This general trend is punctuated by eight cooling events on the decadal- to centennial-scale, centered at 0.4, 2.0, 3.7, 5.3, 5.8, 8.3, 9.0, and 9.6 ka B.P. (Figure 4, 5).

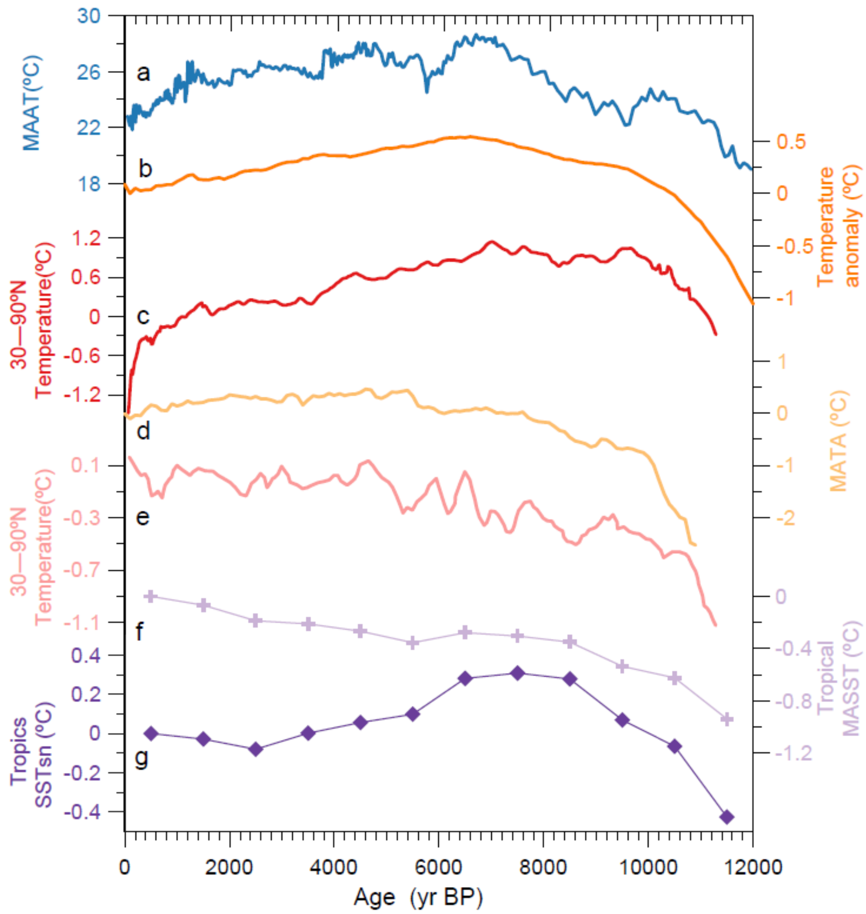

Figure 4. Comparison of the Holocene brGDGTs-based MAAT record with temperature reconstructions and model simulations. (**a**) BrGDGTs-based MAAT from Huguangyan Maar Lake (this study); (**b**) Global mean surface temperature (Temp12k; Kaufman et al., 2020); (**c**) Proxy-based mean temperature of the Northern Hemisphere (90º–30º N; Marcott et al., 2013); (**d**) Pollen-based mean annual temperature anomaly (MATA) for North America and Europe (Marsicek et al., 2018); (**e**) Model-based simulation of the temperature of the Northern Hemisphere (90º–30 ºN; Liu et al., 2014); (**f**) Seasonally-unadjusted SST record (SST_{SN}, 23.5º–23.5ºN; Bova et al., 2021); (**g**) Tropical mean annual SST record (MASST, 23.5ºS–23.5ºN; Bova et al., 2021).

Spectral analysis of the brGDGTs-based temperature series since 8.0 ka BP revealed several statistically significant quasi-periodicities, from the multi-decadal to the centennial scale: 201-202, 111-112, 95-96, 92-93, 78-82, and 64-65 years. Several of these periodicities are close to those of significant solar cycles, such as the

Gleissberg cycle (˜70–100 yr) and the de Vries cycle (˜200-210 yr), although the latter is less significant in the time series (see Supplementary Figure S2).

The record from Maar Lake Huguangyan is indicative of regional-scale temperature change. A comparison of the record with subcontinental and hemispheric temperature time series is shown in Figure 4. In terms of general trends, the brGDGTs-based MAAT record shows a decreasing trend similar to that of global mean surface temperature (Temp12k; Kaufman et al., 2020), and proxy-based mean temperature in the Northern Hemisphere (90º-30ºN; Marcott et al., 2013), but it is in conflict with model simulations of the temperature of the Northern Hemisphere (90º-30 ºN; Liu et al., 2014) and of tropical mean annual sea surface temperature (MASST, 23.5ºS-23.5ºN; Bova et al., 2021). Thus, the Holocene temperature evolution at Huguangyan Maar Lake contrasts with the results of model simulations. One of the reasons for this may be the existence of a model simulation bias in SST reconstructions and uncertainty in the weighting of different forcings.

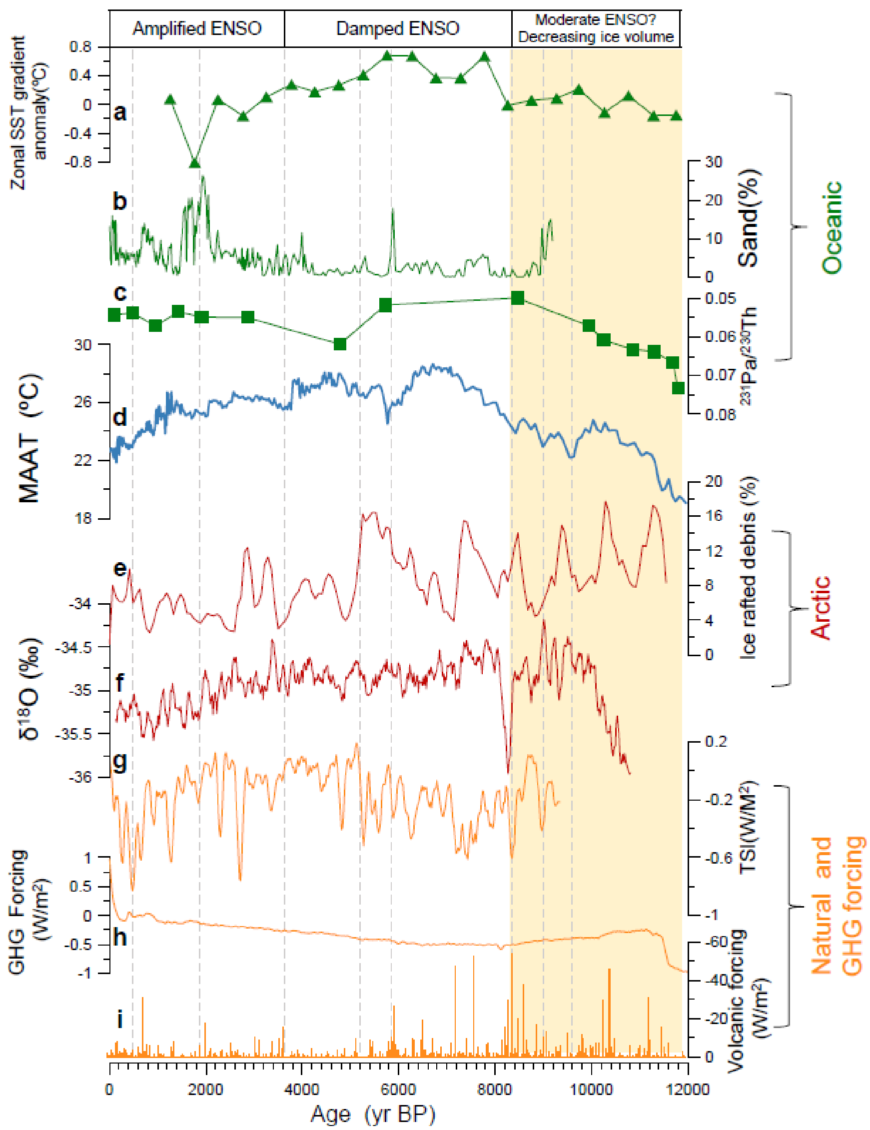

Figure 5. Comparison of the Holocene brGDGTs-based MAAT record from Huguangyan Maar Lake with potential independent internal and external drivers of climate change. (**a**) Zonal SST gradient anomaly

relative to the late Holocene calculated as the difference between the western and eastern Pacific (Koutavas and Joanides, 2012); (**b**) ENSO record from Lake El Junco in the Galápagos Islands (Conroy et al., 2008); (**c**) Sedimentary record of^{231}Pa/^{230}Th from the subtropical North Atlantic Ocean (McManus et al., 2004); (**d**) brGDGTs-based MAAT record from Huguangyan Maar Lake (the data for 10–20 kyr BP are from Chu et al., 2017); (**e**) Ice rafted debris record from North Atlantic sediment cores (Bond et al., 2001); (**f**) Greenland δ^{18}O ice core record (GRIP,11-point running average) (Vinther et al., 2006); (**g**) Record of total solar irradiance (TSI; Steinhilber et al., 2012); (**h**) Record of GHG radiative forcing (CO_2, CH_4, N_2O) (Köhler et al., 2017); (**i**) Record of Volcanic forcing from a Greenland ice core (Kobashi et al., 2017).

The MAAT at Huguangyan Maar Lake can potentially help understand the dynamical origin of both gradual and abrupt Holocene temperature changes. Widely accepted potential drivers of climate change include fluctuations of ice volume or ice sheet dynamics, external drivers such as solar and volcanic activity, ocean circulation (e.g., involving North Atlantic Deep Water, Antarctic Bottom Water, and ENSO), polar sea ice, and atmospheric greenhouse gases (GHG).

Our results suggest that ice volume or ice sheet dynamics suppressed any other forcings and controlled the regional temperature evolution from the last glacial maximum to the early Holocene (8.2 ka BP; Figure 4, 5). GHG radiative forcing (CO2, CH4, N2O; Köhler et al., 2017) may be a secondary factor. Several previous studies have highlighted the importance of ice-sheet dynamics as a driver of temperature change (Baker et al., 2017; Liu et al., 2014; Marsicek et al., 2018). For example, the δ^{18}O record from Kinderlinskaya cave in the Ural Mountains, which is interpreted as a winter temperature proxy (Baker et al., 2017), reveals negative δ^{18}O anomalies at 11.0 and 8.2 ka BP, which could be caused by the effects of enhanced meltwater influx from melting Northern Hemisphere ice sheets on North Atlantic Ocean circulation (Baker et al., 2017).

Changes in North Atlantic Deep Water (NADW), Atlantic Meridional Overturning Circulation (AMOC), and Antarctic Bottom Water (ABW) have been suggested as major causes of abrupt climate changes (McManus et al., 2004; Struve et al., 2020). Both the AMOC (McManus et al., 2004) and Antarctic Bottom Water (UCDW and AAIW) show a pronounced shift in the middle Holocene (Figure 5), and the distinct temperature shift at ˜5.8 ka BP evident in the MAAT record from Huguangyan Maar Lake could be related to this major change in oceanic circulation.

El Niño–Southern Oscillation (ENSO) variability and the ENSO mode (e.g., EP, CP) may significantly influence both SSTs and temperature changes in some terrestrial regions. Generally, El Niño is significantly positively correlated with winter air temperature variability, especially in the case of the negative temperature anomalies in eastern China during the EP La Niña phase (Ren et al., 2020; Wang et al., 2017). An amplified ENSO in the late Holocene and a damped ENSO during the middle Holocene have also been recognized (Carré et al., 2014; Conroy et al., 2008; Koutavas & Joanides, 2012), although their long-term linkage with climate in China is unclear.

Sea ice extent in the Arctic and Antarctic has been recognized as an important driver of abrupt climatic change on both interannual to annual timescales. The influence of sea ice on abrupt climatic events on decadal to centennial timescales via the amplification of sea-ice-albedo feedbacks, deep-water formation, and shifts of the Intertropical Convergence Zone (e.g., Bond et al., 2001; Moros et al., 2006) are also recognized. Bond et al. (2001) attributed abrupt Holocene climatic events recorded in marine sediment cores and other paleoclimatic records to the effects of changes in solar activity on sea ice extent via amplification and transmission processes involved in ocean-atmosphere circulation. However, the variation of sea-ice extent during the Holocene shows a complex pattern or even opposite trends in the Arctic oceans (Moros et al., 2006). Although it remains difficult to accurately reconstruct spatiotemporal changes in sea ice or ice-rafting (Moros et al., 2006), sea ice variability could be one of several important drivers of abrupt climate changes.

Within the limits of the dating uncertainty, most of the cooling events observed in the brGDGTs-based MAAT record can be linked to oceanic and external forcings; however, the effects of the solar minima at ˜2.6, ˜6.2 and ˜7.4 ka BP are less clearly evident (Figure 5). The large temperature variations observed at tropical Huguangyan Maar Lake could also be caused by winter monsoon amplification. In continental

Eurasia, the winter monsoon plays an important role in the amplification and rapid transmission of the temperature signal from the Arctic to the tropics, and in the migration of the intertropical convergence zone(Chu et al., 2017).

3.3 The brGDGTs-based temperature change during the last deglaciation

Previous brGDGTs-based records indicate that the average MAAT was 17.8ºC during the Oldest Dryas, which was followed by a gradual rise during the Bølling-Allerød interstadial, when it reached a maximum of 21.8 at 13.0 ka BP. Subsequently, the average MAAT decreased to 19.5 during the Younger Dryas (Figure 6b; Chu et al., 2017). This temperature pattern strongly suggests the influence of ice volume or ice sheet and meltwater dynamics on the temperature evolution of the Huguangyan Lake region from the Last Glacial Maximum to the early Holocene (Figure 6).

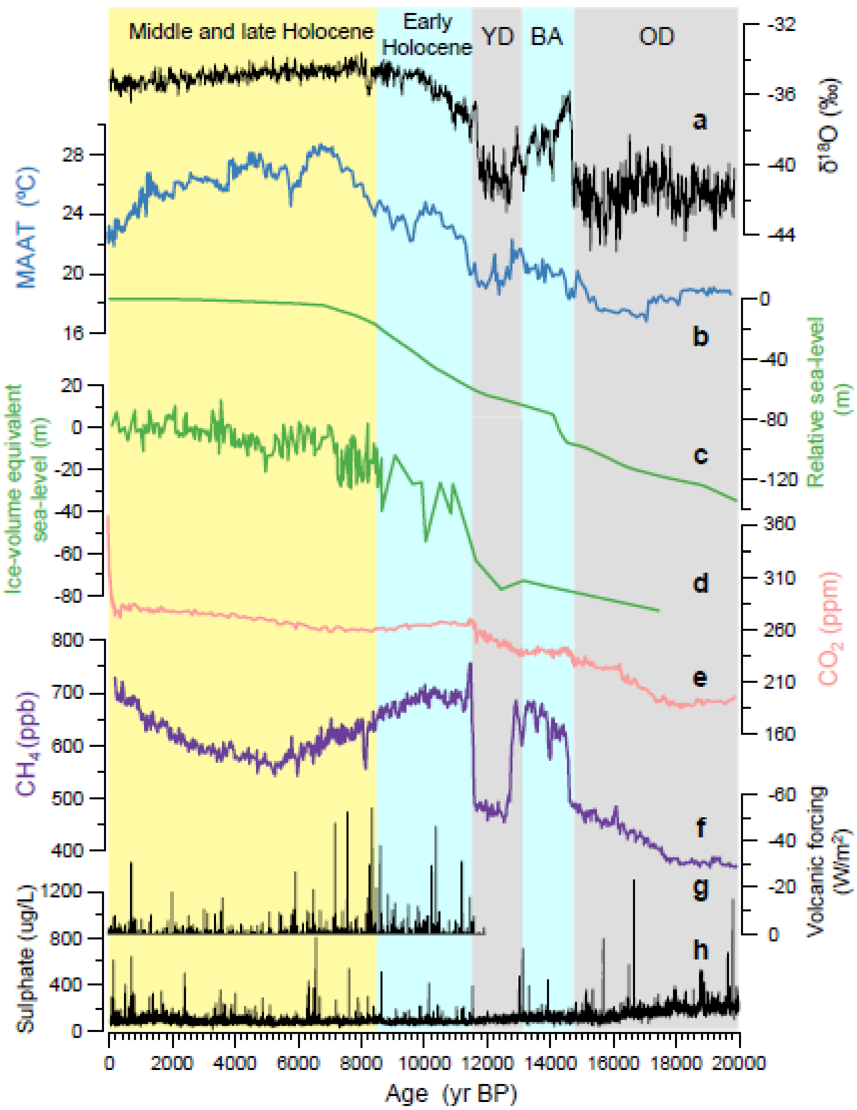

Figure 6. Comparison of the bGDGTs-based MAAT record (this study) with records of ice-volume equivalent sea-level and external climate forcings. (**a**) Greenland $\delta^{18}O$ ice core (GRIP) record (Vinther et al., 2006); (**b**) bGDGTs-based MAAT record from Huguangyan Maar Lake (this study; The data for 10–20 kyr

BP is from Chu et al., 2017); (**c**) Global ice volume record (relative sea level) from Grant et al. (2012); (**d**) Ice-volume equivalent sea-level record (Lambeck et al., 2014); (**e**) Dome C, antarctica, ice core CO_2 record (Bereiter et al., 2015); (**f**) WAIS Divide CH_4 concentration (Fudge et al., 2013); (**g**) Sulfate record of volcanic forcing from a Greenland ice core (Kobashi et al., 2017); (**h**) Sulfate record from the Dome C ice core, Antarctica (Castellano et al., 2004).

The most striking cooling events evident in the brGDGTs-based MAAT record are linked with the abrupt weakening of the tropical summer monsoon (see Supplementary Figure S3). For example, the high-resolution $\delta^{18}O$ record from Klang Cave in the Thai-Malay Peninsula (Chawchai et al., 2021) shows a large increase of 1.5 6.4 to 5.8 ka BP; and the $\delta^{13}C_{27\text{-}35}$record of leaf wax lipids from the annually laminated sediments of Myanmar Maar Lake Twintaung indicates abrupt failures of the tropical monsoon at ˜3.8 and ˜5.8 ka BP (Chu et al., 2020).

4 Conclusions

Our brGDGTs-based temperature record shows an increasing MAAT during the last deglaciation and early Holocene and reached a maximum at ˜6.6 kyr BP, followed by a decrease in middle and late Holocene. It is noted that our temperature reconstruction is in good agreement with instrumental temperature from 2010 CE to 1951 CE. We contend that the last deglaciation and early Holocene temperature variation is linked with the ice volume and/or ice sheet, while the temperature variations during the middle and late Holocene could be ascribed to several possible factors, such as oceanic and atmospheric circulation, and external drivers in Huguangyan Lake region.

Author contributions

Funding acquisition: G. Q. Chu, Q. Sun

Investigation: G. Q. Chu, Z. Y. Zhu, Q. Z. Zhu

Methodology: Q. Li, M. M. Xie, N. Zhan ,Y. Ling

Writing-Original draft: Q. Li, G. Q. Chu, Q. Sun

Writing-reviewing & editing: Q. Li, G. Q. Chu, Q. Sun, M. M. Xie

Acknowledgments

This work was funded by the National Natural Science Foundation of China (Grant 42030507, 41877301), the National Key Research and Development Program of China (Grant 2017YFA0603400) and the Strategic Priority Research Program of the Chinese Academy of Sciences (Grant XDB26000000).

References

Baker, J.L., Lachniet, M.S., Chervyatsova, O., Asmerom, Y. & Polyak, V.J. (2017). Holocene warming in western continental Eurasia driven by glacial retreat and greenhouse forcing. Nature Geoscience, 10(6), 430-435. doi:10.1038/ngeo2953.

Bereiter, B., Eggleston, S., Schmitt, J., Nehrbass-Ahles, C., Stocker, T.F., Fischer, H., et al. (2015). Revision of the EPICA Dome C CO2 record from 800 to 600 kyr before present. Geophysical Research Letters, 42(2), 542-549. doi:10.1002/2014GL061957.

Bond, G., Kromer, B., Beer, J., Muscheler, R., Evans, M.N., Showers, W., et al. (2001). Persistent solar influence on north Atlantic climate during the Holocene. Science, 294(5549), 2130-2136. doi:10.1126/science.1065680.

Bova, S., Rosenthal, Y., Liu, Z., Godad, S.P. & Yan, M. (2021). Seasonal origin of the thermal maxima at the Holocene and the last interglacial. Nature, 589(7843), 548-553. doi:10.1038/s41586-020-03155-x.

Carré, M., Sachs Julian, P., Purca, S., Schauer Andrew, J., Braconnot, P., Falcón Rommel, A., et al. (2014). Holocene history of ENSO variance and asymmetry in the eastern tropical Pacific. Science, 345(6200), 1045-1048. doi:10.1126/science.1252220.

Castellano, E., Becagli, S., Jouzel, J., Migliori, A., Severi, M., Steffensen, J.P., et al. (2004). Volcanic eruption frequency over the last 45 ky as recorded in Epica-Dome C ice core (East Antarctica) and its relationship with climatic changes. Global and Planetary Change, 42(1), 195-205. doi:10.1016/j.gloplacha.2003.11.007.

Chawchai, S., Tan, L., Löwemark, L., Wang, H.-C., Yu, T.-L., Chung, Y.-C., et al. (2021). Hydroclimate variability of central Indo-Pacific region during the Holocene. Quaternary Science Reviews, 253, 106779. doi:10.1016/j.quascirev.2020.106779.

Chu, G., Liu, J., Sun, Q., Lu, H., Wang, W. & Liu, T. (2002). The 'Mediaeval Warm Period' drought recorded in Lake Huguangyan, tropical South China. Holocene, 12, 511-516. doi:10.1191/0959683602hl566ft.

Chu, G., Sun, Q., Zhu, Q., Shan, Y., Shang, W., Ling, Y., et al. (2017). The role of the Asian winter monsoon in the rapid propagation of abrupt climate changes during the last deglaciation. Quaternary Science Reviews, 177, 120-129. doi:10.1016/j.quascirev.2017.10.014.

Chu, G., Zhu, Q., Sun, Q., Su, Y., Xie, M., Zaw, T. & Sein, K. (2020). Drought Cycles Over the Last 8,200 Years Recorded in Maar Lake Twintaung, Myanmar. Journal of Geophysical Research: Atmospheres, 125(9). doi:10.1029/2019jd032225.

Chu, K.S. & Ching, C. (1973), A preliminary study on the climatic fluctuations during the last 5,000 years in China.

Conroy, J.L., Overpeck, J.T., Cole, J.E., Shanahan, T.M. & Steinitz-Kannan, M. (2008). Holocene changes in eastern tropical Pacific climate inferred from a Galápagos lake sediment record. Quaternary Science Reviews, 27(11), 1166-1180. doi:10.1016/j.quascirev.2008.02.015.

Damsté, J.S.S., Ossebaar, J., Abbas, B., Schouten, S. & Verschuren, D. (2009). Fluxes and distribution of tetraether lipids in an equatorial African lake: Constraints on the application of the TEX86 palaeothermometer and BIT index in lacustrine settings. Geochim. Cosmochim. Acta, 73(14), 4232-4249. doi:10.1016/j.gca.2009.04.022.

Damsté, J.S.S., Schouten, S., Hopmans, E.C., van Duin, A.C.T. & Geenevasen, J.A.J. (2002). Crenarchaeol. Journal of Lipid Research, 43(10), 1641-1651. doi:10.1194/jlr.M200148-JLR200.

De Jonge, C., Hopmans, E.C., Zell, C.I., Kim, J.-H., Schouten, S. & Sinninghe Damsté, J.S. (2014). Occurrence and abundance of 6-methyl branched glycerol dialkyl glycerol tetraethers in soils: Implications for palaeoclimate reconstruction. Geochim. Cosmochim. Acta, 141, 97-112. doi:10.1016/j.gca.2014.06.013.

Ding, S., Xu, Y., Wang, Y., He, Y., Hou, J., Chen, L. & He, J.S. (2015). Distribution of branched glycerol dialkyl glycerol tetraethers in surface soils of the Qinghai–Tibetan Plateau: implications of brGDGTs-based proxies in cold and dry regions. Biogeosciences, 12(11), 3141-3151. doi:10.5194/bg-12-3141-2015.

Dutt, S., Gupta, A.K., Clemens, S.C., Cheng, H., Singh, R.K., Kathayat, G. & Edwards, R.L. (2015). Abrupt changes in Indian summer monsoon strength during 33,800 to 5500 years B.P. Geophysical Research Letters, 42(13), 5526-5532. doi:10.1002/2015GL064015.

Fudge, T.J., Steig, E.J., Markle, B.R., Schoenemann, S.W., Ding, Q., Taylor, K.C., et al. (2013). Onset of deglacial warming in West Antarctica driven by local orbital forcing. Nature, 500(7463), 440-444. doi:10.1038/nature12376.

Ge, Q., Zheng, J. & Hao, Z. (2015). PAGES synthesis study on climate changes in Asia over the last 2000 years: Progresses and perspectives. Acta Geographica Sinica, 70(3), 355-363.

Grant, K.M., Rohling, E.J., Bar-Matthews, M., Ayalon, A., Medina-Elizalde, M., Ramsey, C.B., et al. (2012). Rapid coupling between ice volume and polar temperature over the past 150,000 years. Nature, 491(7426), 744-747. 10.1038/nature11593.

Gupta, A.K., Anderson, D.M. & Overpeck, J.T. (2003). Abrupt changes in the Asian southwest monsoon during the Holocene and their links to the North Atlantic Ocean. Nature, 421(6921), 354-357. doi:10.1038/nature01340.

Hopmans, E.C., Weijers, J.W.H., Schefuss, E., Herfort, L., Sinninghe Damste, J.S. & Schouten, S. (2004). A novel proxy for terrestrial organic matter in sediments based on branched and isoprenoid tetraether lipids. Earth and Planetary Science Letters, 224(1), 107-116. doi:10.1016/j.epsl.2004.05.012.

Hu, J., Zhou, H., Peng, P.a. & Spiro, B. (2016). Seasonal variability in concentrations and fluxes of glycerol dialkyl glycerol tetraethers in Huguangyan Maar Lake, SE China: Implications for the applicability of the MBT–CBT paleotemperature proxy in lacustrine settings. Chemical Geology, 420, 200-212. doi:10.1016/j.chemgeo.2015.11.008.

Huguet, C., Smittenberg, R.H., Boer, W., Sinninghe Damste, J.S. & Schouten, S. (2007). Twentieth century proxy records of temperature and soil organic matter input in the Drammensfjord, southern Norway. Organic Geochemistry, 38(11), 1838-1849. doi:10.1016/j.orggeochem.2007.06.015.

Jones, P.D. & Mann, M.E. (2004). Climate over past millennia. Reviews of Geophysics, 42(2). doi:10.1029/2003RG000143.

Kaiser, J., Schouten, S., Kilian, R., Arz, H.W., Lamy, F. & Sinninghe Damste, J.S. (2015). Isoprenoid and branched GDGT-based proxies for surface sediments from marine, fjord and lake environments in Chile. Organic Geochemistry, 89-90, 117-127. doi:10.1016/j.orggeochem.2015.10.007.

Kaufman, D., McKay, N., Routson, C., Erb, M., Datwyler, C., Sommer, P.S., et al. (2020). Holocene global mean surface temperature, a multi-method reconstruction approach. Scientific data, 7(1), 201. doi:10.1038/s41597-020-0530-7.

Kobashi, T., Menviel, L., Jeltsch-Thommes, A., Vinther, B.M., Box, J.E., Muscheler, R., et al. (2017). Volcanic influence on centennial to millennial Holocene Greenland temperature change. Scientific Reports, 7(1), 1441. doi:10.1038/s41598-017-01451-7.

Kohler, P., Nehrbass-Ahles, C., Schmitt, J., Stocker, T.F. & Fischer, H. (2017). A 156 kyr smoothed history of the atmospheric greenhouse gases CO2, CH4, and N2O and their radiative forcing. Earth Syst. Sci. Data, 9(1), 363-387. doi:10.5194/essd-9-363-2017.

Koutavas, A. & Joanides, S. (2012). El Nino–Southern Oscillation extrema in the Holocene and Last Glacial Maximum. Paleoceanography, 27(4). doi:10.1029/2012PA002378.

Lambeck, K., Rouby, H., Purcell, A., Sun, Y. & Sambridge, M. (2014). Sea level and global ice volumes from the Last Glacial Maximum to the Holocene. Proceedings of the National Academy of Sciences, 111(43), 15296. doi:10.1073/pnas.1411762111.

Liu, Z., Zhu, J., Rosenthal, Y., Zhang, X., Otto-Bliesner, B.L., Timmermann, A., et al. (2014). The Holocene temperature conundrum. Proc Natl Acad Sci USA, 111(34), E3501-3505. doi:10.1073/pnas.1407229111.

Loomis, S.E., Russell, J.M., Ladd, B., Street-Perrott, F.A. & Sinninghe Damste, J.S. (2012). Calibration and application of the branched GDGT temperature proxy on East African lake sediments. Earth and Planetary Science Letters, 357-358, 277-288. doi:10.1016/j.epsl.2012.09.031.

Mann, M.E., Cane, M.A., Zebiak, S.E. & Clement, A. (2005). Volcanic and Solar Forcing of the Tropical Pacific over the Past 1000 Years. Journal of Climate, 18(3), 447-456. 10.1175/JCLI-3276.1.

Marcott, S.A., Shakun, J.D., Clark, P.U. & Mix, A.C. (2013). A Reconstruction of Regional and Global Temperature for the Past 11,300 Years. Science, 339(6124), 1198-1201. doi:10.1126/science.1228026.

Marsicek, J., Shuman, B.N., Bartlein, P.J., Shafer, S.L. & Brewer, S. (2018). Reconciling divergent trends and millennial variations in Holocene temperatures. Nature, 554(7690), 92-96. 10.1038/nature25464.

Martin, C., Menot, G., Thouveny, N., Peyron, O., Andrieu-Ponel, V., Montade, V., et al. (2020). Early Holocene Thermal Maximum recorded by branched tetraethers and pollen in Western Europe (Massif Central, France). Quaternary Science Reviews, 228. doi:10.1016/j.quascirev.2019.106109.

McManus, J.F., Francois, R., Gherardi, J.M., Keigwin, L.D. & Brown-Leger, S. (2004). Collapse and rapid resumption of Atlantic meridional circulation linked to deglacial climate changes. Nature, 428(6985), 834-837. 10.1038/nature02494.

Moros, M., Andrews, J.T., Eberl, D.D. & Jansen, E. (2006). Holocene history of drift ice in the northern North Atlantic: Evidence for different spatial and temporal modes. Paleoceanography, 21(2). doi:10.1029/2005PA001214.

Naafs, B.D.A., Inglis, G.N., Zheng, Y., Amesbury, M.J., Biester, H., Bindler, R., et al. (2017). Introducing global peat-specific temperature and pH calibrations based on brGDGT bacterial lipids. Geochim. Cosmochim. Acta, 208, 285-301. doi:10.1016/j.gca.2017.01.038.

Pearson, E.J., Juggins, S., Talbot, H.M., Weckstrom, J., Rosen, P., Ryves, D.B., et al. (2011). A lacustrine GDGT-temperature calibration from the Scandinavian Arctic to Antarctic: Renewed potential for the application of GDGT-paleothermometry in lakes. Geochim. Cosmochim. Acta, 75(20), 6225-6238. doi:10.1016/j.gca.2011.07.042.

Peterse, F., van der Meer, J., Schouten, S., Weijers, J.W.H., Fierer, N., Jackson, R.B., et al. (2012). Revised calibration of the MBT–CBT paleotemperature proxy based on branched tetraether membrane lipids in surface soils. Geochim. Cosmochim. Acta, 96, 215-229. doi:10.1016/j.gca.2012.08.011.

Ray, T.C., Daniel, P.R., Huey, T.L., Lev, S.S. & Winston, H. (1991), Indium tin oxide single-mode waveguide modulator, paper presented at Proc.SPIE.

Ren, M., Zhang, W., Geng, X. & Liu, C. (2020). ENSO impact on the variability of wintertime synoptic-scale air temperature over China and possible mechanisms behind. Acta Meteorologica Sinica, 78(2), 199-209.

Russell, J.M., Hopmans, E.C., Loomis, S.E., Liang, J. & Sinninghe Damste, J.S. (2018). Distributions of 5- and 6-methyl branched glycerol dialkyl glycerol tetraethers (brGDGTs) in East African lake sediment: Effects of temperature, pH, and new lacustrine paleotemperature calibrations. Organic Geochemistry, 117, 56-69. doi:10.1016/j.orggeochem.2017.12.003.

Sanchi, L., Menot, G. & Bard, E. (2014). Insights into continental temperatures in the northwestern Black Sea area during the Last Glacial period using branched tetraether lipids. Quaternary Science Reviews, 84, 98-108. doi:10.1016/j.quascirev.2013.11.013.

Schouten, S., Hopmans, E.C., Pancost, R.D. & Damste, J.S.S. (2000). Widespread occurrence of structurally diverse tetraether membrane lipids: Evidence for the ubiquitous presence of low-temperature relatives of hyperthermophiles. Proceedings of the National Academy of Sciences, 97(26), 14421. doi:10.1073/pnas.97.26.14421.

Schouten, S., Hopmans, E.C. & Sinninghe Damste, J.S. (2013). The organic geochemistry of glycerol dialkyl glycerol tetraether lipids: A review. Organic Geochemistry, 54, 19-61. doi:10.1016/j.orggeochem.2012.09.006.

Schulz, M. & Mudelsee, M. (2002). REDFIT: estimating red-noise spectra directly from unevenly spaced paleoclimatic time series. Computers & Geosciences, 28(3), 421-426. doi:10.1016/S0098-3004(01)00044-9.

Steinhilber, F., Abreu, J.A., Beer, J., Brunner, I., Christl, M., Fischer, H., et al. (2012). 9,400 years of cosmic radiation and solar activity from ice cores and tree rings. Proceedings of the National Academy of Sciences, 109(16), 5967. doi:10.1073/pnas.1118965109.

Struve, T., Wilson, D.J., van de Flierdt, T., Pratt, N. & Crocket, K.C. (2020). Middle Holocene expansion of Pacific Deep Water into the Southern Ocean. Proceedings of the National Academy of Sciences, 117(2), 889. doi:10.1073/pnas.1908138117.

Stuiver, M., Reimer, P.J., Bard, E., Beck, J.W., Burr, G.S., Hughen, K.A., et al. (1998). INTCAL98 Radiocarbon Age Calibration, 24,000–0 cal BP. Radiocarbon, 40(3), 1041-1083. doi:10.1017/S0033822200019123.

Sun, Q., Chu, G., Liu, M., Xie, M., Li, S., Ling, Y., et al. (2011). Distributions and temperature dependence of branched glycerol dialkyl glycerol tetraethers in recent lacustrine sediments from China and Nepal. Journal of Geophysical Research, 116(G1). doi:10.1029/2010jg001365.

Tian, L., Wang, M., Zhang, X., Yang, X., Zong, Y., Jia, G., et al. (2019). Synchronous change of temperature and moisture over the past 50 ka in subtropical southwest China as indicated by biomarker records in a crater lake. Quaternary Science Reviews, 212, 121-134. doi:10.1016/j.quascirev.2019.04.003.

Tierney J.E. & deMenocal Peter, B. (2013). Abrupt Shifts in Horn of Africa Hydroclimate Since the Last Glacial Maximum. Science, 342(6160), 843-846. doi:10.1126/science.1240411.

Tierney, J.E. & Russell, J.M. (2009). Distributions of branched GDGTs in a tropical lake system: Implications for lacustrine application of the MBT/CBT paleoproxy. Organic Geochemistry, 40(9), 1032-1036. doi:10.1016/j.orggeochem.2009.04.014.

Tierney, J.E., Russell, J.M., Eggermont, H., Hopmans, E.C., Verschuren, D. & Sinninghe Damste, J.S. (2010). Environmental controls on branched tetraether lipid distributions in tropical East African lake sediments. Geochim. Cosmochim. Acta, 74(17), 4902-4918. doi:10.1016/j.gca.2010.06.002.

Vinther, B.M., Clausen, H.B., Johnsen, S.J., Rasmussen, S.O., Andersen, K.K., Buchardt, S.L., et al. (2006). A synchronized dating of three Greenland ice cores throughout the Holocene. Journal of Geophysical Research: Atmospheres, 111(D13). doi:10.1029/2005JD006921.

Wang, L., Li, J., Lu, H., Gu, Z., Rioual, P., Hao, Q., et al. (2012). The East Asian winter monsoon over the last 15,000 years: its links to high-latitudes and tropical climate systems and complex correlation to the summer monsoon. Quaternary Science Reviews, 32, 131-142. doi:10.1016/j.quascirev.2011.11.003.

Wang, X., Chu, G., Sheng, M., Zhang, S., Li, J., Chen, Y., et al. (2016). Millennial-scale Asian summer monsoon variations in South China since the last deglaciation. Earth and Planetary Science Letters, 451, 22-30. doi:10.1016/j.epsl.2016.07.006.

Wang, Z., Zhang, W. & Geng, X. (2017). Temporal and spatial variations of the first and last frost dates in China's inland agricultural region from 1961to 2014and their relationships with circulation factors. Acta Meteorologica Sinica, 75(4), 564-580.

Weijers, J.W.H., Schouten, S., van den Donker, J.C., Hopmans, E.C. & Damste, J.S.S. (2007). Environmental controls on bacterial tetraether membrane lipid distribution in soils. Geochim. Cosmochim. Acta, 71(3), 703-713. doi:10.1016/j.gca.2006.10.003.

Yancheva, G., Nowaczyk, N.R., Mingram, J., Dulski, P., Schettler, G., Negendank, J.F.W., et al. (2007). Influence of the intertropical convergence zone on the East Asian monsoon. Nature, 445(7123), 74-77. doi:10.1038/nature05431.

Yang, H., Pancost, R.D., Dang, X., Zhou, X., Evershed, R.P., Xiao, G., et al. (2014). Correlations between microbial tetraether lipids and environmental variables in Chinese soils: Optimizing the paleo-reconstructions in semi-arid and arid regions. Geochim. Cosmochim. Acta, 126, 49-69. doi:10.1016/j.gca.2013.10.041.

Yuan, D., Cheng, H., Edwards, R.L., Dykoski, C.A., Kelly, M.J., Zhang, M., et al. (2004). Timing, Duration, and Transitions of the Last Interglacial Asian Monsoon. Science, 304(5670), 575-578. doi:10.1126/science.1091220.

Zink, K.G., Vandergoes, M.J., Bauersachs, T., Newnham, R.M., Rees, A.B.H. & Schwark, L. (2016). A refined paleotemperature calibration for New Zealand limnic environments using differentiation of branched glycerol dialkyl glycerol tetraether (brGDGT) sources. Journal of Quaternary Science, 31(7), 823-835. doi:10.1002/jqs.2908.

Hosted file

`supporting information s1.docx` available at https://authorea.com/users/540866/articles/601055-temperature-variations-during-the-past-20-ka-at-huguangyan-maar-lake-in-tropical-china-and-dynamic-link

Qi Li[1,2], Qing Sun[3], Manman Xie[3], Yuan Ling[4], Zeyang Zhu[1], Qingzeng Zhu[1], Nan Zhan[3], Guoqiang Chu[1,5,6]

[1]Institute of Geology and Geophysics, Chinese Academy of Sciences, Beijing 100029, China.

[2] University of Chinese Academy of Sciences, Beijing 100049, China.

[3] National Research Center of Geoanalysis, Beijing 100037, China.

[4] Institute of Geology, Chinese Academy of Geological Sciences, Beijing 100037, China.

[5] CAS Center for Excellence in Life and Paleoenvironment, Beijing 100044, China.

[6] Innovation Academy for Earth Science, Chinese Academy of Sciences, Beijing 100029, China.

Corresponding author:

G. Chu (chuguoqiang@mail.igcas.ac.cn) and Q. Sun (sunqing1616@yahoo.com)

Key Points:

- A temperature record over last 20 ka from Huguangyan Maar Lake in tropical China based on brGDGTs
- The Holocene temperature evolution at Huguangyan Maar Lake characterized with a regional-scale temperature change
- Ice volume may be main driving force on the temperature change of Huguangyan Maar Lake region from the Last Glacial Maximum to Holocene

Abstract

Discrepancies exist in global temperature evolution from the Last Glacial Maximum to the present between model simulations and proxy reconstruction. This debate is critical for understanding and evaluating current global warming on a longer timescale. Here we report a branched GDGTs-based temperature reconstruction from the sediments of Huguangyan Maar Lake in southeast China and validate it using historical documentary evidence and instrumental data. The reconstructed mean annual air temperature (MAAT) indicates distinct changes during the last deglaciation (Oldest Dryas, Bølling-Allerød, Younger Dryas). During the Holocene, temperatures gradually increased from the end of the Younger Dryas to ~7.0 ka BP, followed by a decrease in recent decades. However, our terrestrial temperature record differs with model simulations and proxy sea surface temperature records of the Holocene. We conclude that ice volume or ice sheet is the most prominent forcing that controlled the regional temperature evolution from the Last Glacial Maximum to the beginning of the middle Holocene; while the temperature variations during the middle and late

Holocene were mainly regulated by several possible factors, such as oceanic and atmospheric circulation, and external drivers (solar and volcanic activity).

1 Introduction

There is an ongoing debate about the Holocene temperature record of the extratropical Northern Hemisphere. Proxy records show a general long-term cooling trend since the early Holocene (Marcott et al., 2013), while model simulations indicate a warming trend over the past ~12,000 years (Liu et al., 2014). Models play an important role in understanding how climate systems respond to various forcing factors and boundary conditions. However, many dynamic processes are not well computed or weighted in the model simulations, such as external forcing factors (solar irradiance and explosive volcanism), and the internal variability of the climate system (e.g., ENSO, PDO, AO, and the monsoon). Moreover, proxy-based temperature reconstructions are often of low resolution and have relatively large uncertainties in proxy calibration and dating, as well as regional or seasonal biases. Hence, more regional proxy-based paleoclimate time series are needed to verify the climatic record of the Holocene and to understand the differences between model simulations and paleoclimate reconstructions.

In this study, we present a high resolution branched glycerol dialkyl glycerol tetraethers (brGDGTs) membrane lipids-based temperature reconstruction (0-10 ka BP) combined with previously published data (10-20 ka BP) from the sediments of Huguangyan Maar Lake (21º9´N, 110º17´E) in tropical China (Chu et al., 2017), with the aim of obtaining a regional terrestrial temperature record and to understand its dynamic links.

Our paleotemperature proxy is based on brGDGTs, which comprise two dialkyl chains with different amounts of methyl and cyclopentane moieties (Damsté et al., 2009; Hopmans et al., 2004; Naafs et al., 2017; Sanchi et al., 2014; Schouten et al., 2000; Schouten et al., 2013; Sun et al., 2011; Tierney & Russell, 2009; Weijers et al., 2007). The physical and biological mechanisms of the temperature sensitivity of brGDGTs could be due to their membrane components maintaining membrane fluidity via methyl and cyclopentane moieties (Damsté et al., 2002; Huguet et al., 2007; Weijers et al., 2007). The methylation index of branched tetraethers (MBT) and the cyclization ratio of branched tetraethers (CBT) have previously been used to reconstruct terrestrial paleotemperatures from lacustrine sediments, soils, and peat sequences (Ding et al., 2015; Naafs et al., 2017; Peterse et al., 2012; Weijers et al., 2007; Yang et al., 2014).

Numerous studies have confirmed that brGDGTs-based indices from lacustrine sediments can be used to reconstruct terrestrial paleotemperatures (De Jonge et al., 2014; Hu et al., 2016; Kaiser et al., 2015; Loomis et al., 2012; Martin et al., 2020; Naafs et al., 2017; Pearson et al., 2011; Russell et al., 2018; Sun et al., 2011; Tian et al., 2019; Tierney et al., 2010; Weijers et al., 2007; Zink et al., 2016). However, several interpretational uncertainties remain, such as regarding the relative contributions of aquatic sources and soil sources to brGDGTs because the calibration functions from soils and lakes are quite different. Huguangyan

Lake is a small, hydrologically-closed lake with no inflows and a small watershed area, and therefore the sedimentary organic matter originates mainly in the water column (Chu et al., 2017; Hu et al., 2016). The within-lake origin of the sedimentary organic matter, which is also supported by the relatively low sedimentary TOC/N ratios since ~20 ka BP (Chu et al., 2002), substantially reduces this source of uncertainty in paleotemperature reconstruction. Previous brGDGTs-based MAAT reconstructions during the last deglaciation from the sediments of Huguangyan Maar Lake demonstrated a distinctive pattern of temperature changes from during the Oldest Dryas, Bølling-Allerød, Younger Dryas, and the onset of the Holocene (Chu et al., 2017).

2 Materials and Methods

2.1 Study site

Maar lakes are recognized as ideal sites for preserving high-resolution sedimentary archives because they are closed basins with a relatively simple hydrological system and they provide continuous sedimentary sequences (Yancheva et al., 2007). Huguangyan Maar Lake is a closed basin without stream inputs located in the Leizhou Peninsula in the tropical region of South China. The surface area is 2.3 km2, the maximum water depth is 22 m, and the watershed area is 3.2 km2 (Figure 1) (Chu et al., 2002; Yancheva et al., 2007). The area has a mean annual air temperature of 23.4℃ and a temperature difference between winter and summer of 11.9℃ (1964–2004; data from Zhanjiang meteorological station). Overlapping piston cores were collected from near the center of the lake in a water depth of 14 m. The cores were sliced at a 1-cm interval and then freeze dried for GDGTs extraction.

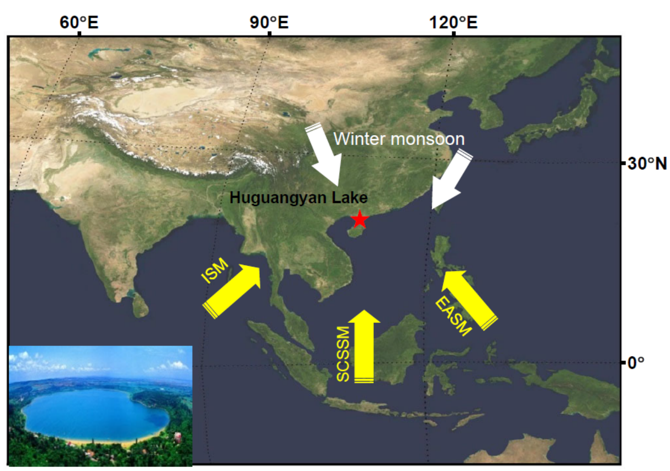

Figure 1. Location of Huguangyan Maar Lake. Solid arrows indicate the dominant direction of the summer monsoon (yellow) and winter monsoon (white). The inset photo shows Huguangyan Lake. Background image is modified from NASA (http://visibleearth.nasa.gov).

2.2 Chronology

The sedimentary chronology for Huguangyan Maar Lake is based on 14 AMS ^{14}C dates from handpicked leaves and/or other terrestrial plant macrofossils, together with analyses of ^{137}Cs and ^{210}Pb concentrations (Table 1; Figure 2; Supplementary Figure S1). The results of radiometric dating (^{137}Cs, ^{210}Pb, AMS^{14}C) have been presented previously (Chu et al., 2017; Wang et al., 2016).

Table 1. Radiocarbon ages from Huguangyan Maar Lake.

Lab. code	**Material**	**Depth (cm)**	**Radiocarbon age (BP)**	**Calibrated age (Median)**
Poz-47119	Leaves	53	850±40	738
Poz-47120	Leaves	94	1200±50	1135
Poz-47121	Branch	135	1275±30	1233
Poz-47122	Leaves	179	1875±35	1822
Poz-47187	Leaves	290	3650±35	3941
Poz-47123	Leaves	399	4140±40	4644
Poz-47124	Leaves	541	6280±40	7215
Poz-47188	Leaves	626	9420±80	10640
Poz-47125	Leaves	671	10300±70	12246
Poz-47127	Leaves	731	11430±60	13427
Poz-47128	Leaves	815	13420±70	16122
Poz-47129	Charcoal	882	14530±170	17399
Poz-47130	Charcoal	936	15590±120	18619
Poz-47131	Charcoal	1026	16980±200	20219

All AMS ^{14}C ages were calibrated using the atmospheric data set from the calibration program CALIB 4.3 (Stuiver et al., 1998).

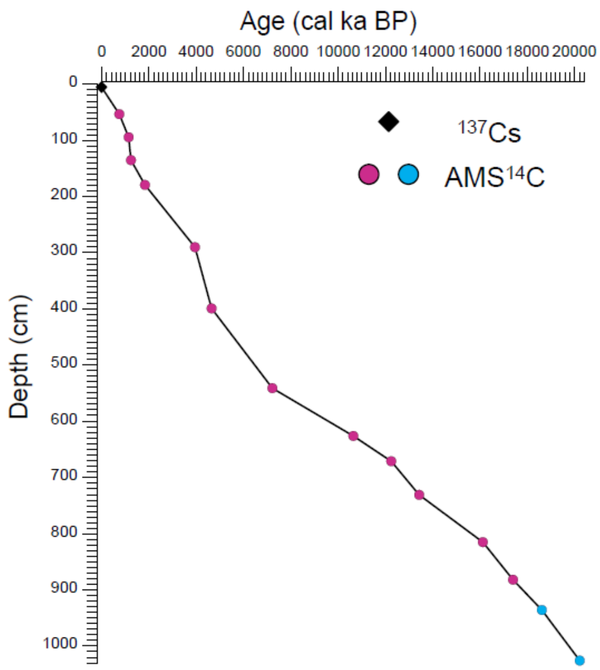

Figure 2. Age-depth plot for the Maar Lake Huguangyan. The calibrated AMS14C dates are from Wang et al., (2016) (red) and Chu et al., (2017) (blue).

2.3 GDGTs analysis

This study builds upon previous work of Huguangyan Maar Lake (Chu et al., 2017). For GDGTs analysis, freeze-dried samples (~1.5 g) were extracted using a dichloromethane (DCM): methanol (9:1, v/v) mixture with an accelerated solvent extractor (ASE 350) at 120 ℃ and 1500 psi for two cycles. The extracts were dried under N_2 and separated into apolar and polar fractions over an activated Al2O3 column using hexane: DCM (9:1, v/v) and DCM: methanol (1:1, v/v) as the respective eluents.

The branched GDGTs were analyzed using a Shimadzu high-performance liquid chromatography triple quadrupole mass spectrometry system (HPLC-MS), with an autosampler and Analyst software (modified by Hopmans et al., 2004; Weijers et al., 2007). Separation was achieved using a Grace Prevail Cyano column (150 mm × 2.1 mm; 3 m); ion scanning was performed in a single ion monitoring mode at m/z 1050, 1048, 1046, 1036, 1034, 1032, 1022, 1020 and 1018. The brGDGTs were quantified using a C46 internal standard.

MAAT from brGDGT for the Huguangyan Maar Lake was obtained using the degree of methylation (MBT) and the cyclisation ration of branched tetraether (CBT) according to the proxy calibration for the lacustrine sediment from China and Nepal (Sun et al., 2011):

$$MAAT=3.949 - 5.593 \times CBT + 38.213 \times MBT \ (n=100, r^2=0.73)$$

3 Result and Discussion

3.1 Reconstruction temperature vs. instrumental data and historical documentary.

All proxy data are indirect measurements of climate change, and therefore it is necessary to calibrate or validate them against instrumental or other independent data(Jones & Mann, 2004). Hence, we compared the brGDGTs-based MAAT record from Huguangyan Maar Lake with several other independent climate datasets: instrumental annual mean air temperature data from Zhanjiang meteorological station, ~15 km from Huguangyan Lake; historical documents from 140 local chronicles and 14 monographs from southern China (south of 23.5ºN), and a synthetic temperature reconstruction for China (Figure 3c).

The reconstructed MAAT is 22.5°C for the period of 2010 CE–1951 CE (based on 137Cs-dating of the uppermost part of the sediment column). This result is close to the instrumental annual mean air temperature (23.2°C) for the same period obtained from nearby Zhanjiang meteorological station, however, there is a 0.7°C offset between the instrumental data and the reconstructed temperatures. Although temperatures in this tropical lake are favorable for biological activity throughout the year, the brGDGTs-based temperature is slightly biased to winter and spring temperatures because of the turnover of the water column, which causes nutrient-rich bottom water to reach the surface and support the growth of aquatic organisms. This was confirmed by the seasonal flux of brGDGTs estimated from sediment traps (Hu et al., 2016), together with monthly observations of planktonic diatoms (Wang et al., 2012). The occurrence of lower temperatures during the 1970s is confirmed by both instrumental data for 1921 CE–1939 CE and 1951 CE–2010 CE, as well as by the MAAT reconstruction (Figure 3a).

Historical documents have often been used for paleoclimatic reconstruction. In tropical China, historical documents are widely available and there are hundreds of local chronicles. Direct descriptions using terms such as “rivers frozen” and “snow, sleet and frost” in tropical China (south of 23º30’ N) are interpreted as clear evidence of cold events. These abnormal phenomena are related to cold surges (cold waves). Meteorologically, a cold surge has been defined as a very large temperature decrease (exceeding 8°C) within 24 hours, and they are proposed as a surrogate for winter monsoon strength in China (Ray et al., 1991). Cold surges have a relatively short duration, often less than one week. We used historical documents to produce a compilation of evidence of “rivers frozen, snow, sleet and frost in the tropical plains” (south of 23.5º N; see Supplementary Table S1). The sources are from ”Natural disasters in historical documents in Guangdong province” (including Hainan province) and ”Natural disasters in historical documents in Guangxi province” (Institute of Literary and History, Guangdong Province, unpublished data), which consist of 140 local chronicles and 14 monographs.

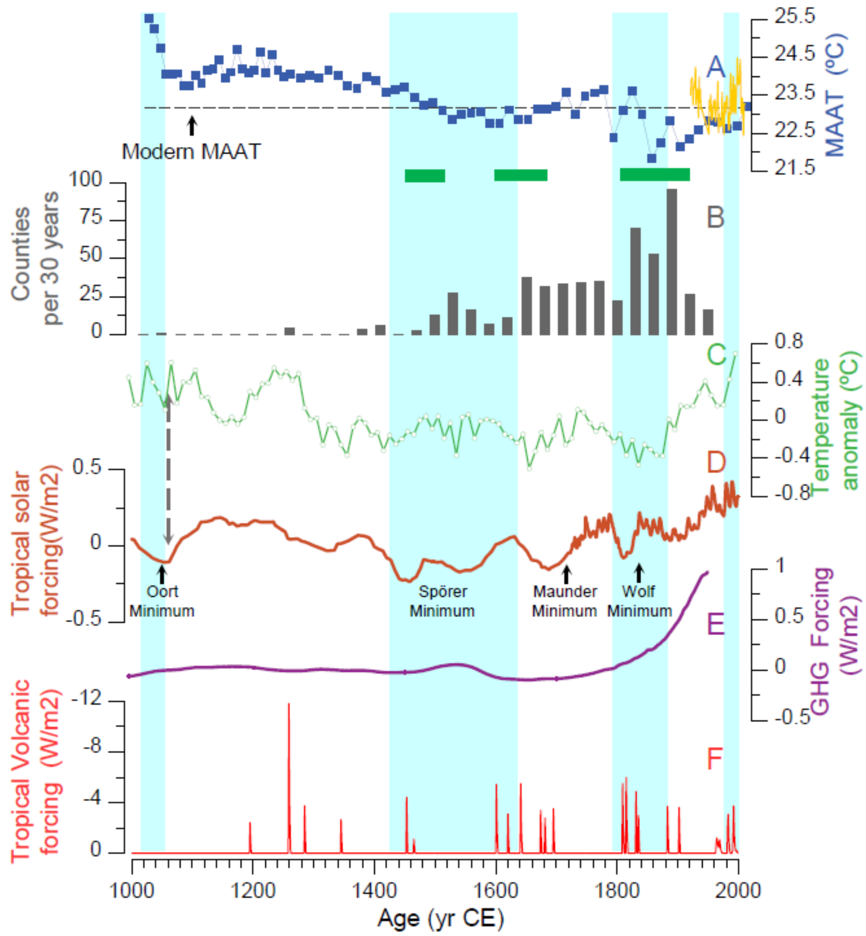

Figure 3. Comparison of the brGDGTs-based MAAT record for Huguangyan Maar Lake with historical documentary evidence, instrumental data, and possible climate forcings during the last millennium. (**a**) brGDGTs-based MAAT record obtained in this study (blue line); annual mean air temperature from Zhangjiang Station (1921–1939 and 1951–2010) (yellow line); modern MAAT for the study area (green dashed line). (**b**) Number of counties with cold surges per 30 years in tropical China years from historical documents; (**c**) Synthetic temperature reconstruction for China (Ge et al., 2015); (**d**) Record of tropical solar forcing (Mann et al., 2005); (**e**) record of GHG radiative forcing (CO_2, CH_4, N_2O) (Köhler et al., 2017); (**f**) Record of tropical volcanic forcing (Mann et al., 2005); Green bars represent the extreme cold winters based on historical documentary evidence from China (Chu and Ching, 1973).

Extreme cold events are concentrated in the Little Ice Age, especially between 800 CE and 1900 CE, while the Medieval Warm Period (MWP) had few fewer cold events (Figure 3b). Historical records are less abundant and intermittent before 1400 CE but are more continuous after the Ming Dynasty (the Fang Zhi (local chronic) period of 1400 CE-1900 CE). The brGDGTs-based MAAT record from Huguangyan Maar Lake shows three cold intervals: 440 CE-1640 CE, 1800 CE-1890 CE, and during the 1970s (Figure 3a). Within the limits of the dating uncertainties, these intervals are consistent with the documentary evidence (Figure 3b).

Natural climate forcings such as changes in solar output and volcanic eruptions are widely recognized as causes of decadal-to-centennial–scale climatic variations. Figure 3 shows that most of the cold intervals recorded at Huguangyan Maar Lake correspond to sunspot minima and episodes of intensified volcanic activity. However, the decrease in MAAT at ~1740 CE is not linked to these forcings.

3.2 Holocene brGDGTs-based temperature change

Although the climate of the Holocene, the most recent interval of Earth history, was more stable than that during the last glacial period, it was interrupted by several abrupt cooling events on the decadal- to centennial-scale (Bond et al., 2001). The brGDGTs-based temperature record from Huguangyan Maar Lake shows an increase in MAAT from 22℃ after the Younger Dryas (11.5 ka BP) to 28℃ by ~7.0 ka BP, followed by a gradual decrease from 23.5℃ in recent decades. This general trend is punctuated by eight cooling events on the decadal- to centennial-scale, centered at 0.4, 2.0, 3.7, 5.3, 5.8, 8.3, 9.0, and 9.6 ka B.P. (Figure 4, 5).

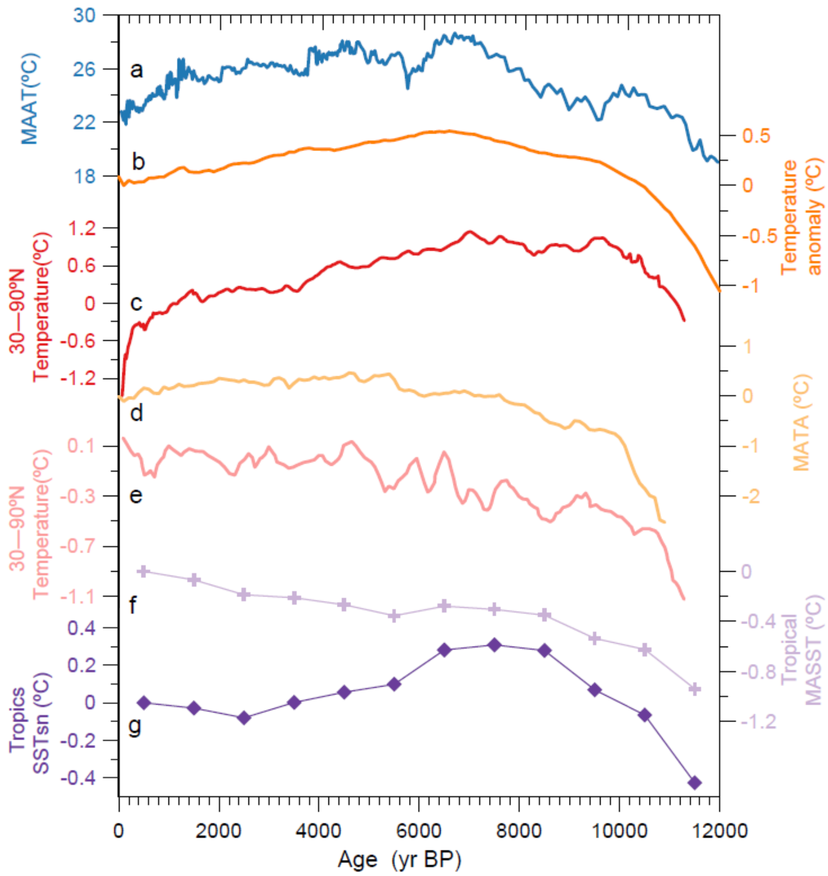

Figure 4. Comparison of the Holocene brGDGTs-based MAAT record with temperature reconstructions and model simulations. (**a**) BrGDGTs-based MAAT from Huguangyan Maar Lake (this study); (**b**) Global mean surface temperature (Temp12k; Kaufman et al., 2020); (**c**) Proxy-based mean temperature of the Northern Hemisphere (90º–30º N; Marcott et al., 2013); (**d**) Pollen-based mean annual temperature anomaly (MATA) for North America and Europe (Marsicek et al., 2018); (**e**) Model-based simulation of the temperature of the Northern Hemisphere (90º–30 ºN; Liu et al., 2014); (**f**) Seasonally-unadjusted SST record (SST_{SN}, 23.5º–23.5ºN; Bova et al., 2021); (**g**) Tropical mean annual SST record (MASST, 23.5ºS–23.5ºN; Bova et al., 2021).

Spectral analysis of the brGDGTs-based temperature series since 8.0 ka BP revealed several statistically significant quasi-periodicities, from the multi-decadal to the centennial scale: 201-202, 111-112, 95-96, 92-93, 78-82, and 64-65 years. Several of these periodicities are close to those of significant solar cycles, such as the Gleissberg cycle (~70–100 yr) and the de Vries cycle (~200-210 yr), although the latter is less significant in the time series (see Supplementary Figure S2).

The record from Maar Lake Huguangyan is indicative of regional-scale temperature change. A comparison of the record with subcontinental and hemispheric temperature time series is shown in Figure 4. In terms of general trends, the brGDGTs-based MAAT record shows a decreasing trend similar to that of global mean surface temperature (Temp12k; Kaufman et al., 2020), and proxy-based mean temperature in the Northern Hemisphere (90º-30ºN; Marcott et al., 2013), but it is in conflict with model simulations of the temperature of the Northern Hemisphere (90º-30 ºN; Liu et al., 2014) and of tropical mean annual sea surface temperature (MASST, 23.5ºS-23.5ºN; Bova et al., 2021). Thus, the Holocene temperature evolution at Huguangyan Maar Lake contrasts with the results of model simulations. One of the reasons for this may be the existence of a model simulation bias in SST reconstructions and uncertainty in the weighting of different forcings.

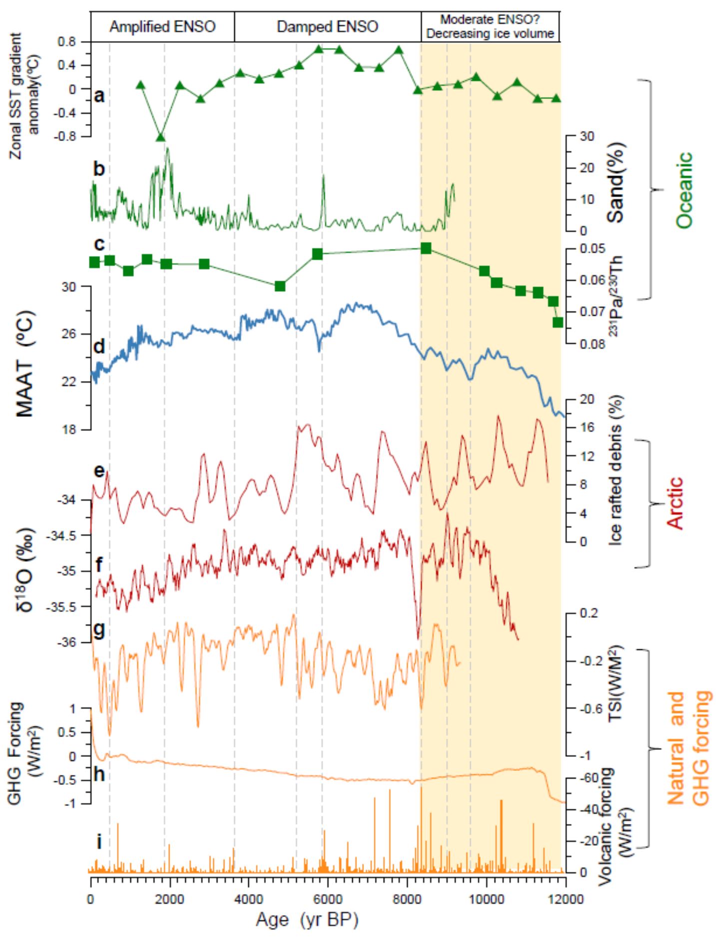

Figure 5. Comparison of the Holocene brGDGTs-based MAAT record from Huguangyan Maar Lake with potential independent internal and external drivers

of climate change. (**a**) Zonal SST gradient anomaly relative to the late Holocene calculated as the difference between the western and eastern Pacific (Koutavas and Joanides, 2012); (**b**) ENSO record from Lake El Junco in the Galápagos Islands (Conroy et al., 2008); (**c**) Sedimentary record of $^{231}Pa/^{230}Th$ from the subtropical North Atlantic Ocean (McManus et al., 2004); (**d**) brGDGTs-based MAAT record from Huguangyan Maar Lake (the data for 10–20 kyr BP are from Chu et al., 2017); (**e**) Ice rafted debris record from North Atlantic sediment cores (Bond et al., 2001); (**f**) Greenland ^{18}O ice core record (GRIP,11-point running average) (Vinther et al., 2006); (**g**) Record of total solar irradiance (TSI; Steinhilber et al., 2012); (**h**) Record of GHG radiative forcing (CO_2, CH_4, N_2O) (Köhler et al., 2017); (**i**) Record of Volcanic forcing from a Greenland ice core (Kobashi et al., 2017).

The MAAT at Huguangyan Maar Lake can potentially help understand the dynamical origin of both gradual and abrupt Holocene temperature changes. Widely accepted potential drivers of climate change include fluctuations of ice volume or ice sheet dynamics, external drivers such as solar and volcanic activity, ocean circulation (e.g., involving North Atlantic Deep Water, Antarctic Bottom Water, and ENSO), polar sea ice, and atmospheric greenhouse gases (GHG).

Our results suggest that ice volume or ice sheet dynamics suppressed any other forcings and controlled the regional temperature evolution from the last glacial maximum to the early Holocene (8.2 ka BP; Figure 4, 5). GHG radiative forcing (CO2, CH4, N2O; Köhler et al., 2017) may be a secondary factor. Several previous studies have highlighted the importance of ice-sheet dynamics as a driver of temperature change (Baker et al., 2017; Liu et al., 2014; Marsicek et al., 2018). For example, the ^{18}O record from Kinderlinskaya cave in the Ural Mountains, which is interpreted as a winter temperature proxy (Baker et al., 2017), reveals negative ^{18}O anomalies at 11.0 and 8.2 ka BP, which could be caused by the effects of enhanced meltwater influx from melting Northern Hemisphere ice sheets on North Atlantic Ocean circulation (Baker et al., 2017).

Changes in North Atlantic Deep Water (NADW), Atlantic Meridional Overturning Circulation (AMOC), and Antarctic Bottom Water (ABW) have been suggested as major causes of abrupt climate changes (McManus et al., 2004; Struve et al., 2020). Both the AMOC (McManus et al., 2004) and Antarctic Bottom Water (UCDW and AAIW) show a pronounced shift in the middle Holocene (Figure 5), and the distinct temperature shift at ~5.8 ka BP evident in the MAAT record from Huguangyan Maar Lake could be related to this major change in oceanic circulation.

El Niño–Southern Oscillation (ENSO) variability and the ENSO mode (e.g., EP, CP) may significantly influence both SSTs and temperature changes in some terrestrial regions. Generally, El Niño is significantly positively correlated with winter air temperature variability, especially in the case of the negative temperature anomalies in eastern China during the EP La Niña phase (Ren et al., 2020; Wang et al., 2017). An amplified ENSO in the late Holocene and a damped ENSO during the middle Holocene have also been recognized (Carré et al., 2014; Conroy et al., 2008; Koutavas & Joanides, 2012), although their long-term linkage with climate in China is unclear.

Sea ice extent in the Arctic and Antarctic has been recognized as an important driver of abrupt climatic change on both interannual to annual timescales. The influence of sea ice on abrupt climatic events on decadal to centennial timescales via the amplification of sea-ice-albedo feedbacks, deep-water formation, and shifts of the Intertropical Convergence Zone (e.g., Bond et al., 2001; Moros et al., 2006) are also recognized. Bond et al. (2001) attributed abrupt Holocene climatic events recorded in marine sediment cores and other paleoclimatic records to the effects of changes in solar activity on sea ice extent via amplification and transmission processes involved in ocean-atmosphere circulation. However, the variation of sea-ice extent during the Holocene shows a complex pattern or even opposite trends in the Arctic oceans (Moros et al., 2006). Although it remains difficult to accurately reconstruct spatiotemporal changes in sea ice or ice-rafting (Moros et al., 2006), sea ice variability could be one of several important drivers of abrupt climate changes.

Within the limits of the dating uncertainty, most of the cooling events observed in the brGDGTs-based MAAT record can be linked to oceanic and external forcings; however, the effects of the solar minima at ~2.6, ~6.2 and ~7.4 ka BP are less clearly evident (Figure 5). The large temperature variations observed at tropical Huguangyan Maar Lake could also be caused by winter monsoon amplification. In continental Eurasia, the winter monsoon plays an important role in the amplification and rapid transmission of the temperature signal from the Arctic to the tropics, and in the migration of the intertropical convergence zone(Chu et al., 2017).

3.3 The brGDGTs-based temperature change during the last deglaciation

Previous brGDGTs-based records indicate that the average MAAT was 17.8ºC during the Oldest Dryas, which was followed by a gradual rise during the Bølling-Allerød interstadial, when it reached a maximum of 21.8℃ at 13.0 ka BP. Subsequently, the average MAAT decreased to 19.5℃ during the Younger Dryas (Figure 6b; Chu et al., 2017). This temperature pattern strongly suggests the influence of ice volume or ice sheet and meltwater dynamics on the temperature evolution of the Huguangyan Lake region from the Last Glacial Maximum to the early Holocene (Figure 6).

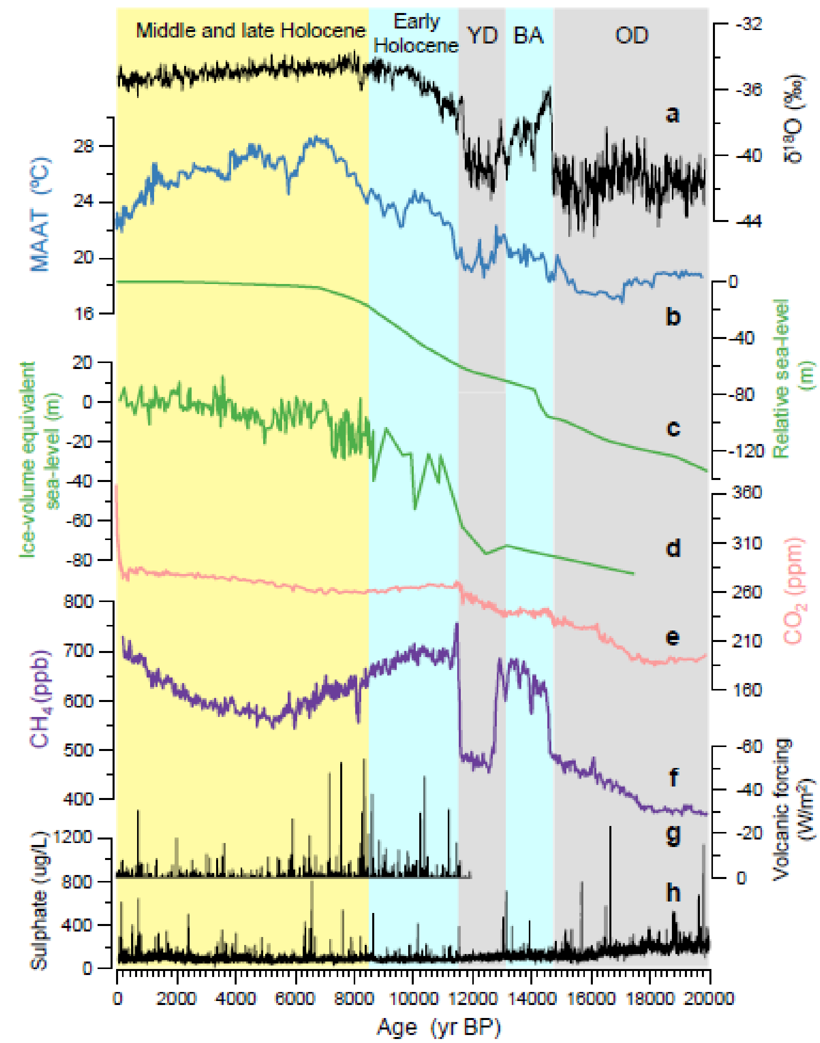

Figure 6. Comparison of the bGDGTs-based MAAT record (this study) with records of ice-volume equivalent sea-level and external climate forcings. (**a**) Greenland ^{18}O ice core (GRIP) record (Vinther et al., 2006); (**b**) bGDGTs-based MAAT record from Huguangyan Maar Lake (this study; The data for 10–20 kyr BP is from Chu et al., 2017); (**c**) Global ice volume record (relative sea level) from Grant et al. (2012); (**d**) Ice-volume equivalent sea-level record (Lambeck et al., 2014); (**e**) Dome C, antarctica, ice core CO_2 record (Bereiter et al., 2015); (**f**) WAIS Divide CH_4 concentration (Fudge et al., 2013); (**g**) Sulfate record of volcanic forcing from a Greenland ice core (Kobashi et al., 2017); (**h**) Sulfate record from the Dome C ice core, Antarctica (Castellano et al., 2004).

The most striking cooling events evident in the brGDGTs-based MAAT record are linked with the abrupt weakening of the tropical summer monsoon (see Supplementary Figure S3). For example, the high-resolution ^{18}O record from Klang Cave in the Thai-Malay Peninsula (Chawchai et al., 2021) shows a large increase of 1.5 ‰ from 6.4 to 5.8 ka BP; and the $^{13}C_{27\text{-}35}$ record of leaf wax lipids from the annually laminated sediments of Myanmar Maar Lake Twintaung indicates abrupt failures of the tropical monsoon at ~3.8 and ~5.8 ka BP (Chu et al., 2020).

4 Conclusions

Our brGDGTs-based temperature record shows an increasing MAAT during the last deglaciation and early Holocene and reached a maximum at ~6.6 kyr BP, followed by a decrease in middle and late Holocene. It is noted that our temperature reconstruction is in good agreement with instrumental temperature from 2010 CE to 1951 CE. We contend that the last deglaciation and early Holocene temperature variation is linked with the ice volume and/or ice sheet, while the temperature variations during the middle and late Holocene could be ascribed to several possible factors, such as oceanic and atmospheric circulation, and external drivers in Huguangyan Lake region.

Author contributions

Funding acquisition: G. Q. Chu, Q. Sun

Investigation: G. Q. Chu, Z. Y. Zhu, Q. Z. Zhu

Methodology: Q. Li, M. M. Xie, N. Zhan ,Y. Ling

Writing-Original draft: Q. Li, G. Q. Chu, Q. Sun

Writing-reviewing & editing: Q. Li, G. Q. Chu, Q. Sun, M. M. Xie

Acknowledgments

This work was funded by the National Natural Science Foundation of China (Grant 42030507, 41877301), the National Key Research and Development Program of China (Grant 2017YFA0603400) and the Strategic Priority Research Program of the Chinese Academy of Sciences (Grant XDB26000000).

References

Baker, J.L., Lachniet, M.S., Chervyatsova, O., Asmerom, Y. & Polyak, V.J. (2017). Holocene warming in western continental Eurasia driven by glacial retreat and greenhouse forcing. Nature Geoscience, 10(6), 430-435. doi:10.1038/ngeo2953.

Bereiter, B., Eggleston, S., Schmitt, J., Nehrbass-Ahles, C., Stocker, T.F., Fischer, H., et al. (2015). Revision of the EPICA Dome C CO2 record from 800 to 600 kyr before present. Geophysical Research Letters, 42(2), 542-549. doi:10.1002/2014GL061957.

Bond, G., Kromer, B., Beer, J., Muscheler, R., Evans, M.N., Showers, W., et al. (2001). Persistent solar influence on north Atlantic climate during the Holocene.

Science, 294(5549), 2130-2136. doi:10.1126/science.1065680.

Bova, S., Rosenthal, Y., Liu, Z., Godad, S.P. & Yan, M. (2021). Seasonal origin of the thermal maxima at the Holocene and the last interglacial. Nature, 589(7843), 548-553. doi:10.1038/s41586-020-03155-x.

Carré, M., Sachs Julian, P., Purca, S., Schauer Andrew, J., Braconnot, P., Falcón Rommel, A., et al. (2014). Holocene history of ENSO variance and asymmetry in the eastern tropical Pacific. Science, 345(6200), 1045-1048. doi:10.1126/science.1252220.

Castellano, E., Becagli, S., Jouzel, J., Migliori, A., Severi, M., Steffensen, J.P., et al. (2004). Volcanic eruption frequency over the last 45 ky as recorded in Epica-Dome C ice core (East Antarctica) and its relationship with climatic changes. Global and Planetary Change, 42(1), 195-205. doi:10.1016/j.gloplacha.2003.11.007.

Chawchai, S., Tan, L., Löwemark, L., Wang, H.-C., Yu, T.-L., Chung, Y.-C., et al. (2021). Hydroclimate variability of central Indo-Pacific region during the Holocene. Quaternary Science Reviews, 253, 106779. doi:10.1016/j.quascirev.2020.106779.

Chu, G., Liu, J., Sun, Q., Lu, H., Wang, W. & Liu, T. (2002). The 'Mediaeval Warm Period' drought recorded in Lake Huguangyan, tropical South China. Holocene, 12, 511-516. doi:10.1191/0959683602hl566ft.

Chu, G., Sun, Q., Zhu, Q., Shan, Y., Shang, W., Ling, Y., et al. (2017). The role of the Asian winter monsoon in the rapid propagation of abrupt climate changes during the last deglaciation. Quaternary Science Reviews, 177, 120-129. doi:10.1016/j.quascirev.2017.10.014.

Chu, G., Zhu, Q., Sun, Q., Su, Y., Xie, M., Zaw, T. & Sein, K. (2020). Drought Cycles Over the Last 8,200 Years Recorded in Maar Lake Twintaung, Myanmar. Journal of Geophysical Research: Atmospheres, 125(9). doi:10.1029/2019jd032225.

Chu, K.S. & Ching, C. (1973), A preliminary study on the climatic fluctuations during the last 5,000 years in China.

Conroy, J.L., Overpeck, J.T., Cole, J.E., Shanahan, T.M. & Steinitz-Kannan, M. (2008). Holocene changes in eastern tropical Pacific climate inferred from a Galápagos lake sediment record. Quaternary Science Reviews, 27(11), 1166-1180. doi:10.1016/j.quascirev.2008.02.015.

Damsté, J.S.S., Ossebaar, J., Abbas, B., Schouten, S. & Verschuren, D. (2009). Fluxes and distribution of tetraether lipids in an equatorial African lake: Constraints on the application of the TEX86 palaeothermometer and BIT index in lacustrine settings. Geochim. Cosmochim. Acta, 73(14), 4232-4249. doi:10.1016/j.gca.2009.04.022.

Damsté, J.S.S., Schouten, S., Hopmans, E.C., van Duin, A.C.T. & Geenevasen, J.A.J. (2002). Crenarchaeol. Journal of Lipid Research, 43(10), 1641-1651. doi:10.1194/jlr.M200148-JLR200.

De Jonge, C., Hopmans, E.C., Zell, C.I., Kim, J.-H., Schouten, S. & Sinninghe Damsté, J.S. (2014). Occurrence and abundance of 6-methyl branched glycerol dialkyl glycerol tetraethers in soils: Implications for palaeoclimate reconstruction. Geochim. Cosmochim. Acta, 141, 97-112. doi:10.1016/j.gca.2014.06.013.

Ding, S., Xu, Y., Wang, Y., He, Y., Hou, J., Chen, L. & He, J.S. (2015). Distribution of branched glycerol dialkyl glycerol tetraethers in surface soils of the Qinghai–Tibetan Plateau: implications of brGDGTs-based proxies in cold and dry regions. Biogeosciences, 12(11), 3141-3151. doi:10.5194/bg-12-3141-2015.

Dutt, S., Gupta, A.K., Clemens, S.C., Cheng, H., Singh, R.K., Kathayat, G. & Edwards, R.L. (2015). Abrupt changes in Indian summer monsoon strength during 33,800 to 5500 years B.P. Geophysical Research Letters, 42(13), 5526-5532. doi:10.1002/2015GL064015.

Fudge, T.J., Steig, E.J., Markle, B.R., Schoenemann, S.W., Ding, Q., Taylor, K.C., et al. (2013). Onset of deglacial warming in West Antarctica driven by local orbital forcing. Nature, 500(7463), 440-444. doi:10.1038/nature12376.

Ge, Q., Zheng, J. & Hao, Z. (2015). PAGES synthesis study on climate changes in Asia over the last 2000 years: Progresses and perspectives. Acta Geographica Sinica, 70(3), 355-363.

Grant, K.M., Rohling, E.J., Bar-Matthews, M., Ayalon, A., Medina-Elizalde, M., Ramsey, C.B., et al. (2012). Rapid coupling between ice volume and polar temperature over the past 150,000 years. Nature, 491(7426), 744-747. 10.1038/nature11593.

Gupta, A.K., Anderson, D.M. & Overpeck, J.T. (2003). Abrupt changes in the Asian southwest monsoon during the Holocene and their links to the North Atlantic Ocean. Nature, 421(6921), 354-357. doi:10.1038/nature01340.

Hopmans, E.C., Weijers, J.W.H., Schefuß, E., Herfort, L., Sinninghe Damsté, J.S. & Schouten, S. (2004). A novel proxy for terrestrial organic matter in sediments based on branched and isoprenoid tetraether lipids. Earth and Planetary Science Letters, 224(1), 107-116. doi:10.1016/j.epsl.2004.05.012.

Hu, J., Zhou, H., Peng, P.a. & Spiro, B. (2016). Seasonal variability in concentrations and fluxes of glycerol dialkyl glycerol tetraethers in Huguangyan Maar Lake, SE China: Implications for the applicability of the MBT–CBT paleotemperature proxy in lacustrine settings. Chemical Geology, 420, 200-212. doi:10.1016/j.chemgeo.2015.11.008.

Huguet, C., Smittenberg, R.H., Boer, W., Sinninghe Damsté, J.S. & Schouten, S. (2007). Twentieth century proxy records of temperature and soil organic matter input in the Drammensfjord, southern Norway. Organic Geochemistry, 38(11), 1838-1849. doi:10.1016/j.orggeochem.2007.06.015.

Jones, P.D. & Mann, M.E. (2004). Climate over past millennia. Reviews of Geophysics, 42(2). doi:10.1029/2003RG000143.

Kaiser, J., Schouten, S., Kilian, R., Arz, H.W., Lamy, F. & Sinninghe Damsté, J.S. (2015). Isoprenoid and branched GDGT-based proxies for surface sediments from marine, fjord and lake environments in Chile. Organic Geochemistry, 89-90, 117-127. doi:10.1016/j.orggeochem.2015.10.007.

Kaufman, D., McKay, N., Routson, C., Erb, M., Dätwyler, C., Sommer, P.S., et al. (2020). Holocene global mean surface temperature, a multi-method reconstruction approach. Scientific data, 7(1), 201. doi:10.1038/s41597-020-0530-7.

Kobashi, T., Menviel, L., Jeltsch-Thömmes, A., Vinther, B.M., Box, J.E., Muscheler, R., et al. (2017). Volcanic influence on centennial to millennial Holocene Greenland temperature change. Scientific Reports, 7(1), 1441. doi:10.1038/s41598-017-01451-7.

Köhler, P., Nehrbass-Ahles, C., Schmitt, J., Stocker, T.F. & Fischer, H. (2017). A 156 kyr smoothed history of the atmospheric greenhouse gases CO2, CH4, and N2O and their radiative forcing. Earth Syst. Sci. Data, 9(1), 363-387. doi:10.5194/essd-9-363-2017.

Koutavas, A. & Joanides, S. (2012). El Niño–Southern Oscillation extrema in the Holocene and Last Glacial Maximum. Paleoceanography, 27(4). doi:10.1029/2012PA002378.

Lambeck, K., Rouby, H., Purcell, A., Sun, Y. & Sambridge, M. (2014). Sea level and global ice volumes from the Last Glacial Maximum to the Holocene. Proceedings of the National Academy of Sciences, 111(43), 15296. doi:10.1073/pnas.1411762111.

Liu, Z., Zhu, J., Rosenthal, Y., Zhang, X., Otto-Bliesner, B.L., Timmermann, A., et al. (2014). The Holocene temperature conundrum. Proc Natl Acad Sci USA, 111(34), E3501-3505. doi:10.1073/pnas.1407229111.

Loomis, S.E., Russell, J.M., Ladd, B., Street-Perrott, F.A. & Sinninghe Damsté, J.S. (2012). Calibration and application of the branched GDGT temperature proxy on East African lake sediments. Earth and Planetary Science Letters, 357-358, 277-288. doi:10.1016/j.epsl.2012.09.031.

Mann, M.E., Cane, M.A., Zebiak, S.E. & Clement, A. (2005). Volcanic and Solar Forcing of the Tropical Pacific over the Past 1000 Years. Journal of Climate, 18(3), 447-456. 10.1175/JCLI-3276.1.

Marcott, S.A., Shakun, J.D., Clark, P.U. & Mix, A.C. (2013). A Reconstruction of Regional and Global Temperature for the Past 11,300 Years. Science, 339(6124), 1198-1201. doi:10.1126/science.1228026.

Marsicek, J., Shuman, B.N., Bartlein, P.J., Shafer, S.L. & Brewer, S. (2018). Reconciling divergent trends and millennial variations in Holocene temperatures. Nature, 554(7690), 92-96. 10.1038/nature25464.

Martin, C., Ménot, G., Thouveny, N., Peyron, O., Andrieu-Ponel, V., Montade, V., et al. (2020). Early Holocene Thermal Maximum recorded by branched tetraethers and pollen in Western Europe (Massif Central, France). Quaternary Science Reviews, 228. doi:10.1016/j.quascirev.2019.106109.

McManus, J.F., Francois, R., Gherardi, J.M., Keigwin, L.D. & Brown-Leger, S. (2004). Collapse and rapid resumption of Atlantic meridional circulation linked to deglacial climate changes. Nature, 428(6985), 834-837. 10.1038/nature02494.

Moros, M., Andrews, J.T., Eberl, D.D. & Jansen, E. (2006). Holocene history of drift ice in the northern North Atlantic: Evidence for different spatial and temporal modes. Paleoceanography, 21(2). doi:10.1029/2005PA001214.

Naafs, B.D.A., Inglis, G.N., Zheng, Y., Amesbury, M.J., Biester, H., Bindler, R., et al. (2017). Introducing global peat-specific temperature and pH calibrations based on brGDGT bacterial lipids. Geochim. Cosmochim. Acta, 208, 285-301. doi:10.1016/j.gca.2017.01.038.

Pearson, E.J., Juggins, S., Talbot, H.M., Weckström, J., Rosén, P., Ryves, D.B., et al. (2011). A lacustrine GDGT-temperature calibration from the Scandinavian Arctic to Antarctic: Renewed potential for the application of GDGT-paleothermometry in lakes. Geochim. Cosmochim. Acta, 75(20), 6225-6238. doi:10.1016/j.gca.2011.07.042.

Peterse, F., van der Meer, J., Schouten, S., Weijers, J.W.H., Fierer, N., Jackson, R.B., et al. (2012). Revised calibration of the MBT–CBT paleotemperature proxy based on branched tetraether membrane lipids in surface soils. Geochim. Cosmochim. Acta, 96, 215-229. doi:10.1016/j.gca.2012.08.011.

Ray, T.C., Daniel, P.R., Huey, T.L., Lev, S.S. & Winston, H. (1991), Indium tin oxide single-mode waveguide modulator, paper presented at Proc.SPIE.

Ren, M., Zhang, W., Geng, X. & Liu, C. (2020). ENSO impact on the variability of wintertime synoptic-scale air temperature over China and possible mechanisms behind. Acta Meteorologica Sinica, 78(2), 199-209.

Russell, J.M., Hopmans, E.C., Loomis, S.E., Liang, J. & Sinninghe Damsté, J.S. (2018). Distributions of 5- and 6-methyl branched glycerol dialkyl glycerol tetraethers (brGDGTs) in East African lake sediment: Effects of temperature, pH, and new lacustrine paleotemperature calibrations. Organic Geochemistry, 117, 56-69. doi:10.1016/j.orggeochem.2017.12.003.

Sanchi, L., Ménot, G. & Bard, E. (2014). Insights into continental temperatures in the northwestern Black Sea area during the Last Glacial period using branched tetraether lipids. Quaternary Science Reviews, 84, 98-108. doi:10.1016/j.quascirev.2013.11.013.

Schouten, S., Hopmans, E.C., Pancost, R.D. & Damsté, J.S.S. (2000). Widespread occurrence of structurally diverse tetraether membrane lipids: Evidence for the ubiquitous presence of low-temperature relatives of hyperthermophiles. Proceedings of the National Academy of Sciences, 97(26), 14421. doi:10.1073/pnas.97.26.14421.

Schouten, S., Hopmans, E.C. & Sinninghe Damsté, J.S. (2013). The organic geochemistry of glycerol dialkyl glycerol tetraether lipids: A review. Organic Geochemistry, 54, 19-61. doi:10.1016/j.orggeochem.2012.09.006.

Schulz, M. & Mudelsee, M. (2002). REDFIT: estimating red-noise spectra directly from unevenly spaced paleoclimatic time series. Computers & Geosciences, 28(3), 421-426. doi:10.1016/S0098-3004(01)00044-9.

Steinhilber, F., Abreu, J.A., Beer, J., Brunner, I., Christl, M., Fischer, H., et al. (2012). 9,400 years of cosmic radiation and solar activity from ice cores and tree rings. Proceedings of the National Academy of Sciences, 109(16), 5967. doi:10.1073/pnas.1118965109.

Struve, T., Wilson, D.J., van de Flierdt, T., Pratt, N. & Crocket, K.C. (2020). Middle Holocene expansion of Pacific Deep Water into the Southern Ocean. Proceedings of the National Academy of Sciences, 117(2), 889. doi:10.1073/pnas.1908138117.

Stuiver, M., Reimer, P.J., Bard, E., Beck, J.W., Burr, G.S., Hughen, K.A., et al. (1998). INTCAL98 Radiocarbon Age Calibration, 24,000–0 cal BP. Radiocarbon, 40(3), 1041-1083. doi:10.1017/S0033822200019123.

Sun, Q., Chu, G., Liu, M., Xie, M., Li, S., Ling, Y., et al. (2011). Distributions and temperature dependence of branched glycerol dialkyl glycerol tetraethers in recent lacustrine sediments from China and Nepal. Journal of Geophysical Research, 116(G1). doi:10.1029/2010jg001365.

Tian, L., Wang, M., Zhang, X., Yang, X., Zong, Y., Jia, G., et al. (2019). Synchronous change of temperature and moisture over the past 50 ka in subtropical southwest China as indicated by biomarker records in a crater lake. Quaternary Science Reviews, 212, 121-134. doi:10.1016/j.quascirev.2019.04.003.

Tierney J.E. & deMenocal Peter, B. (2013). Abrupt Shifts in Horn of Africa Hydroclimate Since the Last Glacial Maximum. Science, 342(6160), 843-846. doi:10.1126/science.1240411.

Tierney, J.E. & Russell, J.M. (2009). Distributions of branched GDGTs in a tropical lake system: Implications for lacustrine application of the MBT/CBT paleoproxy. Organic Geochemistry, 40(9), 1032-1036. doi:10.1016/j.orggeochem.2009.04.014.

Tierney, J.E., Russell, J.M., Eggermont, H., Hopmans, E.C., Verschuren, D. & Sinninghe Damsté, J.S. (2010). Environmental controls on branched tetraether lipid distributions in tropical East African lake sediments. Geochim. Cosmochim. Acta, 74(17), 4902-4918. doi:10.1016/j.gca.2010.06.002.

Vinther, B.M., Clausen, H.B., Johnsen, S.J., Rasmussen, S.O., Andersen, K.K., Buchardt, S.L., et al. (2006). A synchronized dating of three Greenland ice cores throughout the Holocene. Journal of Geophysical Research: Atmospheres, 111(D13). doi:10.1029/2005JD006921.

Wang, L., Li, J., Lu, H., Gu, Z., Rioual, P., Hao, Q., et al. (2012). The East Asian winter monsoon over the last 15,000 years: its links to high-latitudes and tropical climate systems and complex correlation to the summer monsoon. Quaternary Science Reviews, 32, 131-142. doi:10.1016/j.quascirev.2011.11.003.

Wang, X., Chu, G., Sheng, M., Zhang, S., Li, J., Chen, Y., et al. (2016). Millennial-scale Asian summer monsoon variations in South China since the last deglaciation. Earth and Planetary Science Letters, 451, 22-30. doi:10.1016/j.epsl.2016.07.006.

Wang, Z., Zhang, W. & Geng, X. (2017). Temporal and spatial variations of the first and last frost dates in China's inland agricultural region from 1961to 2014and their relationships with circulation factors. Acta Meteorologica Sinica, 75(4), 564-580.

Weijers, J.W.H., Schouten, S., van den Donker, J.C., Hopmans, E.C. & Damste, J.S.S. (2007). Environmental controls on bacterial tetraether membrane lipid distribution in soils. Geochim. Cosmochim. Acta, 71(3), 703-713. doi:10.1016/j.gca.2006.10.003.

Yancheva, G., Nowaczyk, N.R., Mingram, J., Dulski, P., Schettler, G., Negendank, J.F.W., et al. (2007). Influence of the intertropical convergence zone on the East Asian monsoon. Nature, 445(7123), 74-77. doi:10.1038/nature05431.

Yang, H., Pancost, R.D., Dang, X., Zhou, X., Evershed, R.P., Xiao, G., et al. (2014). Correlations between microbial tetraether lipids and environmental variables in Chinese soils: Optimizing the paleo-reconstructions in semi-arid and arid regions. Geochim. Cosmochim. Acta, 126, 49-69. doi:10.1016/j.gca.2013.10.041.

Yuan, D., Cheng, H., Edwards, R.L., Dykoski, C.A., Kelly, M.J., Zhang, M., et al. (2004). Timing, Duration, and Transitions of the Last Interglacial Asian Monsoon. Science, 304(5670), 575-578. doi:10.1126/science.1091220.

Zink, K.G., Vandergoes, M.J., Bauersachs, T., Newnham, R.M., Rees, A.B.H. & Schwark, L. (2016). A refined paleotemperature calibration for New Zealand limnic environments using differentiation of branched glycerol dialkyl glycerol tetraether (brGDGT) sources. Journal of Quaternary Science, 31(7), 823-835. doi:10.1002/jqs.2908.

Year (AD)	Description (Summary)	Location
1049	Heavy snow in Oct.	Cangwu County
1245	Heavy snow on Dec. 1	Yingde City
1245	Heavy snow on Dec. 1	Qingyuan City
1245	Heavy snow in Dec. (3 days)	Foshan City
1245	Heavy snow in Dec.	Dongguan City
1348	Heavy snow in winter	Pingle County
1384	Heavy snow in winter	Mengshan County
1384	Heavy snow	Wuzhou City
1384	Heavy snow	Tengxian County
1384	Heavy snow	Yulin City
1415	Heavy frost in May	Chaozhou City
1415	Snow in winter	Panyu County
1415	Heavy snow in winter	Foshan City
1415	Snow in winter	Dongguan City
1415	Heavy snow in winter	Sihui City
1453	Snow in winter	Liuzhou City
1453	Snow in winter	Laibin City
1459	Heavy snow on lunar Jan. 30	Yizhou District in Hechi City
1481	Heavy snow in winter	Jieyang City
1481	Frost in Mar.	Xingning County
1488	Heavy snow in Winter	Gaoming District in Foshan City
1488	Heavy snow in Winter	Yangchun City
1503	Snow in Mar.	Longchuan County
1504	Snow	Yulin City
1504	Frost in Mar.	Xingning County
1506	Snow in winter	Wanning City
1509	Snow in Winter (Oct.)	Chaoyang District in Shantou City
1510	Lijiang River frozen in Nov.	Guilin City
1510	Heavy snow in Winter (Dec.)	Chaozhou City
1510	Heavy snow in Winter (Dec.)	Chaoan District in Chaozhou City
1510	Heavy snow in Winter (Dec.)	Raoping County
1510	Frost in Winter (Dec.)	Jieyang City
1510	Frost in Feb. and Mar.	Lianjiang City
1512	Yongfujiang River frozen in Nov.	Yongfu County
1512	Lijiang River frozen in Nov.	Lingchuan County
1512	Lijiang River frozen in Nov.	Lingui District in Guilin City
1522	Heavy snow in Dec. and frozen	Qinzhou City
1522	Heavy snow and freezing	Hepu County
1526	Heavy snow and in Dec. and frozen	Hepu County
1526	Heavy snow and in Dec. and frozen	Qinzhou City
1526	Heavy frost in Dec. and frozen	Yizhou District in Hechi City
1532	Heavy snow in Winter and frozen	Lechang City
1532	Heavy snow in Winter and frozen	Qujiang District in Shaoguang City

Year (AD)	Description (Summary)	Location
1532	Heavy snow in Winter and frozen	Wengyuan County
1532	Heavy snow in Winter (Nov.)	Chaozhou City
1532	Heavy snow in Winter (Nov.)	Chaoan District in Chaoyang City
1532	Heavy snow in Winter (Nov.)	Jieyang City
1532	Heavy snow in Winter (Nov.)	Chaoyang District in Shantou City
1532	Heavy snow in Winter (Nov.)	Guishan County
1532	Heavy snow in Winter	Yangchun City
1532	Heavy snow in Winter	Heng County
1533	Heavy snow in Mar.	Yulin City
1533	Heavy snow in Winter	Wuming District in Nanning City
1533	Snow in Winter (Dec.)	Deqing County
1533	Snow in Winter (Dec.)	Fengkai County
1533	frozen in Winter	Longchuan County
1535	Snow in Winter	Gaoming District in Foshan City
1536	Snow in Winter (Dec. and Jan.)	Guishan County
1536	Heavy snow in Winter (Dec.)	Deqing County
1536	Heavy snow in Winter	Gaoming District in Foshan City
1537	Heavy snow in Winter	Guangzhou City
1537	Heavy snow in Winter	Panyu County
1537	Heavy snow in Winter	Foshan City
1537	Heavy snow in Winter	Gaoming District in Foshan City
1542	Heavy snow in Winter	Wuming District in Nanning City
1546	Heavy frost in Dec.	Xingning County
1547	Rain and cold in Spring	Foshan City
1547	Rain and cold in Spring	Shunde District in Foshan City
1547	Rain and cold in Spring	Zhongshan City
1547	Frost, abnormal than past	Gaozhou City
1547	Frost in Sept. and Oct.	Lianjiang City
1548	Heavy frost in Oct.	Gaozhou City
1548	Heavy frost in Nov.	Wuchuan City
1549	Heavy frost and snow in Dec.	Huizhou City
1549	Snow in Dec.	Wuhua County
1549	Snow in Dec.	Boluo County
1549	Heavy frost and snow in Winter (Dec.)	Guishan County
1550	Heavy frost and frozen in Winter	Xingning County
1565	Heavy snow in Oct.	Xingan County
1565	Snow in Oct. 29	Lingchuan County
1570	Heavy snow in Dec.	Foshan City
1570	Sonw in Dec. (2 days)	Longchuan County
1578	Snow in Winter	Xinhui District in Jiangmen City
1578	Heavy snow on Dec. 13	Lingchuan County
1578	Heavy snow in Dec.	Xingan County
1579	Rain and hail in Winter	Xingan County

Year (AD)	Description (Summary)	Location
1579	Snow in Dec.	Lingchuan County
1583	Heavy frost in spring	Xingning County
1584	Snow on Jan. 1 and Feb. 12	Gaoyao District in Zhaoqing City
1584	Heavy snow in Winter	Wuming District in Nanning City
1584	Heavy snow on Dec. 1	Binyang County
1585	Snow in Nov.	Heng County
1590	Heavy frost in Winter	Xingning County
1602	Snow in Winter	Guishan County
1606	Extremely cold in Winter	Qiongshan District in Haikou City
1614	Snow in Winter	Xingning County
1614	Heavy snow in Nov.	Heng County
1615	Heavy snow in Winter	Dapu County and Heping County
1619	Heavy snow in Dec. (Dec. 6-Dec. 9)	Dongguan City, Guangdong City, Foshan City and Yangchun City
1621	Snow in Spring (Feb.)	Gaoyao District in Zhaoqing City
1621	Heavy snow in Mar. (half day)	Yangjiang City
1630	Heavy snow in Winter	Yizhou District in Hechi City District
1634	Heavy snow in from Jan. 30 to Jan. 1	Lechang City
1634	Heavy snow in Winter	Renhua County, Xingning County, Wuhua County, Dapu County
1634	Heavy snow from Feb. 5 to Feb. 8	Qujiang District in Shaoguang City
1634	Heavy snow from Feb. 1 to Feb. 7	Conghua District in Guangzhou City
1635	Heavy snow in Winter	Tengxian County
1636	Heavy snow in Winter	Tengxian County, Huaiji County
1636	Heavy frost and extremely cold	Wuhua County
1636	Heavy frost in Winter (Nov.)	Jieyang City
1636	Heavy frost in Dec.	Huilai County
1637	Heavy snow and frozen in Winter (Dec.)	Gaozhou City, Lufeng City, Haifeng County
1637	Heavy snow in Winter (3 days)	Lingao County
1644	Extremely cold on Mar. 28	Longmen County
1654	Heavy snow in Nov.	Nanning City
1654	Heavy snow in Spring (Mar. 6)	Guangzhou City, Longmen County
1654	Heavy snow in Winter (Dec.)	Fengkai County, Haifeng County
1654	Heavy snow in Winter	Laibin City, Gaozhou City, Xinyi City, Maoming City, Wuchuan City
1655	Snow in Winter	Lingxi City
1655	Heavy snow in Feb.	Longchuan County
1655	Frost	Wuhua County
1655	Heavy frost and rivers frozen from Dec.23 to Dec. 26	Huilai County
1656	Heavy snow (4 days) and ice is very thick	Shaoguan City, Lechang City, Wengyuan County

Year (AD)	Description (Summary)	Location
1656	Heavy snow in Feb.	Guishan County, Longchuan County, Wuhua County, Xingning County, Jieyang City, Fengkai County, Dapu County
1658	Heavy snow in Winter	Huaiji County
1663	Heavy snow in Feb. (3 days)	Shaoguan City, Wengyuan County
1666	Heavy frost in Dec.	Huilai County
1667	Heavy frost in Dec.	Deqing County
1667	Snow in Winter	Guangzhou City, Foshan City, Panyu County
1667	Heavy snow on Jan. 14	Shunde District, Foshan City
1667	Heavy snow on Jan. 15	Longmen County
1673	Heavy snow in Feb. and Mar.	Lianping County
1681	Snow in Sept. and Oct.	Gaoyao District, Zhaoqing City, Maoming City
1681	Snow	Wuchuan City
1681	Heavy snow in Sept.	Qinzhou City, Hepu County
1681	Snow in Sept. and Oct.	Huazhou City
1682	Snow in Winter	Gaozhou City, Maoming City, Huazhou City, Wuchuan City
1683	Snow in Winter	Lingxi City
1683	Heavy snow in Winter	Xingan County
1684	Heavy frost on Jan. 8 and from Jan. 17 to Jan 20	Huilai County
1684	Heavy snow in Winter (about 10 days)	Lianping County
1684	Heavy snow in Winter	Guangzhou City, Panyu County, Foshan City,
1684	Heavy snow in Dec.	Xinyi City
1684	Heavy snow and frozen in Winter	Wenchang City
1684	Rain and frost in Jul.	Lingao County
1684	Snow in Dec.	Qiongshan District, Haikou City
1685	Heavy snow and rivers frozen	Kaiping City
1686	Cold and animals were freeze to death	Chaoyang District, Shantou City
1690	Heavy snow in Nov.	Zhaoping County
1690	Heavy snow in Dec.	Quanzhou County
1690	Heavy snow and rivers frozen in Winter	Lianzhou City, Lianshan County
1690	Heavy snow in Winter	Huaiji County, Fengkai County, Sanshui District in Foshan City
1690	Snow and frost in Dec.	Conghua District in Guangzhou City
1690	Snow in Dec. and Jan.	Xingning City
1690	Heavy snow in Winter	Chaoan District in Chaozhou City
1690	Heavy snow and animals were freeze to death in Winter	Chenghai District in Shantou City, Puning City

Year (AD)	Description (Summary)	Location
1690	Heavy snow in winter	Chaoyang District in Shantou City
1690	Frost in Winter (Dec.)	Lingao County
1691	Heavy snow and rivers frozen in Winter (Dec.)	Lingchuan County
1696	Frost in Autumn (Sept.)	Huizhou City
1696	Cold in Jul. and frost in Sept.	Longchuan County
1698	Heavy snow in Winter	Xinxing County
1700	Heavy snow and rivers frozen for half a month in Dec.	Xingan County
1702	Ice is very thick in Winter	Rongxian County
1702	Heavy snow in Winter (Dec. and Jan.)	Wengyuan County
1702	Heavy snow in Winter	Yangchun City
1703	Heavy snow in Winter	Xinfeng County
1703	Frost damaged arecas in Winter	Haikou City
1708	Heavy frost in Feb. and Mar.	Deqing County
1710	Heavy snow in Spring (Mar.)	Dapu County
1711	Heavy snow in Spring (Feb. 17)	Chaoyang District in Shantou City
1712	Heavy snow in Oct.	Tengxian County
1712	Heavy snow and paddy were damaged in Winter	Luchuan County
1712	Ice formed in Aug.	Rongxian County
1712	Cold in Spring	Dapu County
1712	Snow in Sept.	Fengkai County
1713	Heavy snow in Spring (Feb.)	Chaoan District in Chaozhou City, Jieyang City, Chaoyang District in Shantou City
1713	Extremely cold and animals were freezed to death	Wenchang City
1714	Heavy snow and rivers frozen for ten days	Xingan County
1718	Snow in Spring (Feb.)	Xinxing County
1720	Heavy snow in Spring (Feb.)	Dapu County
1720	Snow in Spring (Feb.)	Xinxing County and Kaiping City
1721	Ice formed in Spring (Feb.)	Dapu County and Sanshui District in Foshan City
1721	Sleet in Spring (Feb. and Mar.)	Chaoan District in Chaozhou City, Chaoyang District in Shantou City, Dapu County
1721	Snow in Spring (Feb.)	Jieyang City
1722	Sleet in Spring (Feb. and Mar.)	Sanshui District in Foshan City
1726	Snow in Winter	Quanzhou County
1728	Sleet in Dec.	Zhaoping County
1728	Heavy snow in Dec.	Debao County, Tengxian County, Cangwu County

Year (AD)	Description (Summary)	Location
1728	Heavy snow in Nov. and Dec.	Lingxi City
1728	Heavy snow in Winter	Xinfeng County
1729	Heavy snow in Spring	Chaoan District in Chaozhou City, Lianping County
1729	Heavy snow in Spring (Feb.)	Jieyang City, Huizhou City, Guishan County, Haifeng County
1729	Heavy snow in Spring (Mar.)	Deqing County
1729	Heavy snow in Dec. and Jan.	Lianjiang City
1737	Heavy snow in Spring (Feb.)	Huizhou City, Guishan County
1737	Heavy snow and arecas were damaged in Winter	Wanning City
1740	Heavy snow in Feb.	Zhaoping County, Fuchuan County, Xingan County, Napo County, Lianzhou City, Lianshan County, Laibin City, Xiangzhou County, Liuzhou City
1741	Sleet in Winter	Fengkai County
1741	Heavy snow in Feb.	Yizhou District in Hechi City
1745	Snow in Winter	Liuzhou City
1749	Heavy snow in Jan. and Feb.	Huaiji County
1750	Ice formed in Nov.	Laibin City
1751	Extremely cold and ice formed in Oct.	Laibin City
1752	Heavy snow in Spring (Feb. and Mar.)	Sihui City
1754	Heavy snow in mid Oct.	Longchuan County
1756	Heavy snow in Dec.	Quanzhou County
1757	Heavy frost in Mar.	Shenzhen City
1757	Heavy frost in Sept. and Oct.	Huizhou City, Guishan County
1758	Heavy snow in Feb.	Cangwu County, Fengshun County, Raoping County, Fengkai County
1758	Snow in Feb.	Boluo County, Panyu District in Guangzhou City, Foshan City, Shunde District in Foshan City
1758	Extremely cold and heavy frost in Spring (3 days)	Wanning City
1759	Heavy snow in Dec.	Zhaoping City
1761	Sleet in Dec.	Lingshan County
1762	Heavy snow in Jan.	Longchuan County
1763	Heavy frost in Oct.	Wanning City
1766	Heavy snow in Winter	Mashan County
1767	Heavy snow in Winter	Binyang County
1767	Heavy frost and paddy were damaged in Winter	Wanning City
1768	Heavy snow in Dec.	Tengxian County, Rongxian County
1768	Heavy snow on Oct. 24	Cangwu County, Yulin City

Year (AD)	Description (Summary)	Location
1768	Heavy frost and paddy were damaged in Oct. and Nov,	Longchuan County
1768	Heavy frost in Nov. and Dec.	Wanning City
1769	Heavy frost in Dec.	Yangshan County
1776	Heavy snow on Mar. 7	Jieyang City
1776	Frost in Jul.	Haifeng County
1777	Extremely cold in Jan.	Xinfeng County
1780	Snow and Cold on Dec. 3	Longchuan County
1781	Snow in Feb.	Shunde District in Foshan City
1782	Heavy snow in Winter	Xinfeng County
1783	Rain and cold in Spring	Guishan County, Huizhou City
1784	Heavy frost and paddy were damaged	Longchuan County
1787	Snow for several days in late Mar.	Qingyuan City
1788	Heavy frost and rivers frozen in Winter	Lingshan County
1788	Heavy snow in Spring	Xingning City
1788	Heavy snow in Mar.	Dapu County, Longchuan County
1788	Heavy snow in late Mar.	Qingyuan City, Sanshui District in Foshan City
1789	Heavy snow in Feb.	Mashan County
1794	Frost in Autumn	Heping County
1797	Strong wind and extremely cold on Aug. 8	Longmen County
1800	Heavy snow in Feb.	Shanglin County, Binyang County
1803	Heavy snow on Jan. 23	Yangshan County
1808	Frost and rivers frozen in Oct.	Lingshan County
1809	Heavy snow in Winter	Guangzhou City, Zhaoqing City
1809	Heavy snow in Jan. and Feb.	Yangshan County
1813	Heavy snow in Winter	Tengxian County
1814	Heavy snow in Winter	Tengxian County, Yizhou District in Hechi City, Lianzhou City
1814	Snow in Winter	Shanglin County, Binyang County
1814	Heavy snow and ice formed in Winter	Fengkai County
1815	Snow and rivers frozen in Winter	Yizhou District in Hechi City
1815	Heavy snow in Winter	Lianjiang City
1815	Heavy snow and arecas were damaged in Dec.	Chengmai County
1815	Rain (about 10 days), cold and paddy were damaged in Winter	Haikou City
1815	Heavy snow in Dec. (3 days)	Jingxi City
1815	Heavy snow in Winter	Lipu City
1819	Heavy snow in Nov. (3 days)	Yizhou District in Hechi City
1819	Heavy snow on Nov. 22 and Nov.23	Guiping City, Luocheng County
1819	Heavy snow in Dec. and Jan.	Heping County
1819	Heavy snow in Nov.	Binyang County

Year (AD)	Description (Summary)	Location
1820	Heavy snow in Feb.	Xiangzhou City
1823	Heavy frost and crops were damaged	Longchuan County
1830	Heavy snow and extremely cold on Feb. 8	Dapu County
1831	Heavy frost and paddy were damaged in Oct.	Xingning City
1831	Snow and cold in Winter	Longmen County
1831	Cold in Winter	Sihui City
1831	Snow and extremely cold in Winter	Foshan City
1831	Extremely cold in Winter	Shunde District in Foshan City
1831	Heavy snow in Feb.	Xiangzhou City
1832	Extremely cold in Dec.	Qinzhou City
1832	Heavy snow in Winter	Xingan County, Mengshan County
1832	Heavy snow in Feb. and Nov.	Yingde City
1832	Snow in Spring and heavy frost in Sept.	Xingning City
1832	Frost in Sept. and Oct. and Snow in Dec. and Jan.	Longmen County
1832	Heavy frost in Autumn and heavy snow in Winter (3 days)	Longchuan County
1832	Heavy frost and paddy were damaged in Autumn	Wuhua County
1832	Heavy snow in late Dec. and mid Jan.	Renhua County
1832	Heavy snow in Winter	Lianzhou City
1832	Heavy snow in Dec. and Jan.	Fengkai County
1833	Heavy snow in Jan. and Feb.	Qingyuan City
1833	Heavy snow and ice formed from Jan. 24 to Feb. 4	Heshan City
1833	Snow and cold in Winter	Foshan City, Xingning City
1833	Heavy snow in Winter	Xinfeng County
1835	Heavy snow in Winter	Cangwu County
1835	Heavy snow in Nov.	Lingshan County
1835	Heavy snow on Dec. 16	Tengxian County
1835	Heavy snow on Dec. 20	Guiping City
1835	Heavy snow in Nov.	Beiliu City, Rongxian County, Luchuan County
1835	Heavy snow in Jan.	Yulin City, Sihui City
1836	Snow in Winter	Hepu County, Huizhou City
1836	Heavy snow in Winter	Wuhua County, Deqing County
1836	Heavy snow in Jan. and Feb.	Gaoyao Distirct in Zhaoqing City
1836	Heavy snow in Feb.	Guangzhou City, Longmen County, Panyu District in Guangzhou City, Foshan City, Shunde District in Guangzhou City,Zhongshan City
1836	Heavy snow in Winter	Gaoming District in Foshan City
1836	Heavy snow and strong wind in Feb.	Heshan City

Year (AD)	Description (Summary)	Location
1836	Heavy snow in Winter	Enping City
1836	Heavy snow in Jan. and Feb.	Taishan City, Yangchun City
1837	Snow in Winter	Guiping City, Puning City
1837	Heavy snow in Winter	Pingnan County
1838	Heavy snow in Dec. and Jan.	Longchuan County
1839	Heavy snow on Jan. 13	Kaiping City
1840	Snow in Winter (7 days)	Longchuan County
1840	Heavy snow and extremely cold on Dec. 22	Jieyang City
1846	Heavy snow in Dec.	Cangwu County
1846	Heavy snow on Dec. 15	Guilin City
1846	Heavy snow in Winter	Lianzhou City, Lianshan County
1846	Heavy snow from Dec. 6 to Dec. 8	Yizhou District in Hechi City
1847	Heavy snow and ice formed in Dec.	Guanyang County
1847	Heavy frost and exetremely cold in Jan. and Feb.	Haikou City
1852	Heavy frost and exetremely cold on Dec. 26	Heyuan City
1852	Heavy frost in Dec.	Haikou City
1853	Heavy snow in Winter	Gaoming District in Foshan City
1854	Heavy snow in Dec. and Jan.	Gaozhou City
1855	Heavy snow in Dec.	Pingnan County
1855	Snow in Spring (Feb.)	Xingning City
1856	Snow in Spring (Feb.)	Xingning City
1856	Frost and melon were damaged on Mar, 1	Haifeng County
1856	Extremely cold and river frozen on Feb. 29	Foshan City, Shunde District in Foshan City, Heshan City
1856	Heavy snow in Feb.	Maoming City, Wuchuan City
1856	Frost and cold in late Feb.	Wenchang City
1858	Snow on Feb. 24; rain and hail on Mar. 3	Nanhai District in Foshan City
1859	Rain and cold on Feb. 3	Nanhai District in Foshan City
1859	Rain and cold in Spring	Zhongshan City
1861	Heavy snow in Dec.	Guilin City
1862	Heavy snow in Feb.	Beiliu City, Yulin City, Luchuan County
1862	Heavy snow and ice formed in Feb. and Nov.	Yingde City
1862	Heav snow in Feb.	Raoping County, Guilin City
1862	Extremely cold and ice formed on Jan. 30	Wuchuan City
1862	Snow in Spring	Dianbai District in Maoming City
1862	Extremely cold from Jan. 20 to Feb. 8	Haikou City
1863	Heavy snow and crops were damaged in Winter	Wuchuan City
1864	Heavy snow in Feb.	Lingshan County
1864	Ice formed in Nov.	Pingnan County
1864	Heavy snow in Winter	Laibin City

Year (AD)	Description (Summary)	Location
1864	Heavy snow in Feb. (5 days)	Qujiang District in Shaoguang City, Yingde City, Raoping County, Longchuan County
1864	Snow in Feb.	Qingyuan City
1864	Extremely cold and animals were freezed to death	Maoming City, Wuchuan City
1864	Heavy snow and crops were damaged in Spring	Lianjiang City
1865	Heavy snow in Feb.	Lingshan County
1865	Heavy snow in Dec.	Tengxian County
1865	Sleet for about one month	Quanzhou County
1865	Heavy snow in Feb.	Beiliu City, Luchuan County, Yulin City
1865	Heavy snow in Winter	Laibin City
1866	Heavy snow on Jan. 7	Luoding City
1868	Heavy snow on Dec. 30 and Dec. 31	Sihui City
1868	Heavy snow on Dec. 31	Shunde District in Foshan City, Zhongshan City
1870	Heavy frost and snow in Dec. and Jan.	Raoping County
1871	Snow in Winter	Beiliu City
1871	Heavy snow in Dec. and Jan.	Zhongshan City
1871	Heavy snow and cold in Winter	Raoping County
1871	Frost and crops were damaged in Winter	Haifeng County
1872	Snow in Jan.	Xinyi City
1872	Heavy snow in Jan.	Wuchuan City
1872	Heavy snow in Winter	Huazhou City
1873	Heavy snow in Dec.	Guilin City, Guixian County
1873	Heavy snow in Winter	Laibin City
1874	Heavy snow in Winter	Mengshan County
1874	Haevy snow in Dec.	Laibin City
1875	Snow in Nov.	Luchuan County, Beiliu City
1875	Heavy snow in Nov.	Laibin City
1876	Heavy snow in Jan.	Luoding City
1877	Heavy snow in Jan.	Lingshan County
1877	Heavy snow in Winter	Beiliu City, Luchuan County
1877	Rain from Jan. 12 to Apr. 20	Wenchang City
1877	Snow from Nov. to Feb. next year	Renhua County
1878	Heavy snow and ice formed in Jan.	Qujiang District in Shaoguang City
1878	Snow, hail and cold for about 2 month	Dongguan City, Shunde District in Guangdong City, Heshan City, Enping City
1878	Heavy snow and crops were damaged in Jan.	Wuchuan City
1878	Heavy snow in Feb.	Renhua County
1878	Rain and cold in Feb. (about 10 days)	Haikou City

Year (AD)	Description (Summary)	Location
1878	Snow in Dec. and Jan.	Wuchuan City
1881	Heavy snow and ice formed in Feb.	Guangyang County
1881	Heavy snow and crops were damaged in Dec. and Jan.	Wuchuan City
1882	Heavy snow and crops were damaged in Dec.	Wuchuan City
1883	Heavy snow in Winter	Mengshan County
1886	Heavy snow in late Dec.	Yingde City
1887	Heavy snow in Dec.	Tengxian County, Hexian County, Laibin City
1887	Heavy snow in Winter	Yangshan County, Longchuan County, Deqing County
1888	Heavy snow in Feb.	Beiliu City, Jieyang City
1891	Heavy snow in Jan.	Longchuan County, Hexian County
1892	Heavy snow and ice formed in Nov.	Qinzhou City, Hepu County, Lingshan County, Tengxian County, Hexian County, Beiliu City, Luchuan County, Rongxian County, Guixian County, Guiping City, Yulin City
1892	Heavy snow and animals were freeze to death in Winter	Lipu City
1892	Extremely cold and ice formed in Nov. (about 10 days)	Laibin City
1892	Heavy snow in Nov. (3 days)	Xiangzhou City
1892	Cold in Feb.	Enping City
1892	Snow and Bulls were freeze to death	Qingyuan City
1893	Heavy snow and sugarcane were damaged in Winter	Lechang City
1893	Heavy snow in Jan.	Shixing County, Yangshan County
1893	Heavy snow and arecas were damaged in Jan.	Yingde City
1893	Heavy snow in Jan.	Heping County, Longchuan County
1893	Heavy snow in Winter	Huaiji County, Sihui City, Deqing County, Panyu District and Shunde District in Guangzhou City
1893	Snow on Jan. 14 and heavy snow on Jan. 15 and Jan. 16	Qingyuan City
1893	Heavy rain and ice formed on Jan. 15	Zengcheng District in Guangzhou City
1893	Heavy snow in Jan.	Longmen County, Gaoyao District in Zhaoqing City, Foshan City, Yangchun City
1893	Heavy snow in Jan. (3 days)	Boluo County, Gaoming District in Foshan City

Year (AD)	Description (Summary)	Location
1893	Heavy frost and heavy snow in Winter	Huiyang District in Huizhou City
1893	Heavy snow and animals were freeze to death in Winter	Dapu County, Yunan County
1893	Ice formed and animals were freeze to death in Jan. and Feb.	Fengshun County, Chaoan District in Chaozhou City
1893	Heavy snow in Jan. and Feb.	Luoding City
1893	Heavy snow on Jan. 4 and Jan. 5	Dongguan City
1893	Heavy snow on Jan. 15 and Jan. 16	Zhongshan City, Enping City, Taishan City
1893	Heavy snow on Jan. 15	Kaiping City
1893	Heavy snow on Jan. 16	Lianjiang City
1893	Heavy rain and ice formed on Jan. 7 and Jan. 8	Taishan City
1893	Rain, hail and ice formed on Jan. 14 (3 days)	Yangjiang City
1893	Heavy rain and frost in Jan.	Qiongshan District in Haikou City
1895	Snow on Feb. 21, hail on Mar.4 , frost on Mar. 12 and Sept. 16	Guilin City
1895	Heavy snow in Feb.	Hepu County
1895	Snow and crops were damaged in Sept.	Zhaoping City
1896	Extremely cold on Mar. 19	Wuchuan City
1899	Heavy snow from Dec. 5 to Dec. 7	Guilin City
1900	Heavy snow in Feb.	Xiangzhou City
1901	Heavy snow on Feb. 4	Luoding City
1903	Heavy snow in Nov.	Zhaoping City
1903	Snow and ice formed in Dec.	Longchuan County
1909	Heavy snow in Dec.	Zhaoping City
1911	Snow in late Oct.	Tengxian County
1914	Heavy snow on Dec. 3	Beiliu City
1916	Cold and heavy snow in Spring, the lowest temperature was 1.1℃	Guangzhou City
1916	Heavy snow on Dec. 13	Heping County
1917	Cold and heavy snow in Winter, the lowest temperature was 1.1℃	Guangzhou City
1917	Frost in Jan.	Longchuan County
1918	Frost in Jan. (6 days), the lowest temperature was 1.1℃	Guangzhou City
1919	Heavy snow on Feb. 3	Dapu County
1919	Heavy snow in Feb.	Heping County, Longchuan County
1919	Snow on Feb. 3	Qingyuan City
1919	The lowest temperature was 1.1℃ on Feb. 4	Guangzhou City
1920	Heavy snow in Feb., Mar., and Dec.	Yangshan County
1921	Snow on Jan. 19	Qingyuan City
1923	Heavy snow in Winter	Yangshan County

Year (AD)	Description (Summary)	Location
1924	Cold in Dec.	Longchuan County
1927	Snow in Mar. and frost in Sept.	Longchuan County
1929	Snow in Winter	Tengxian County
1930	Snow on Dec. 21	Shaoguan City
1930	Snow from Dec. 21 to Dec. 23, the lowest temperature was about 4 .4℃	Guangzhou City
1930	Heavy snow in Nov.	Longchuan County
1930	Cold and ice formed in Winter, the temperarure was 0℃	Laibin City
1930	Heavy snow in Feb.	Nanxiong City, Shixing County, Lechang City, Wengyuan County
1930	Heavy snow in Jan. and Feb. and temperature was -1.1℃;	Lianping County, Longchuan County, Heping County
1930	Extremely cold and animals were freezed to death	Guangzhou City
1930	Heavy snow on Jan. 20 and temperature was -1.1℃	Sanshui District in Foshan City
1930	Sleet in Jan. and temperature was 1.1℃	Jiangmen City
1931	Heavy snow on Dec. 13	Nanxiong City
1931	Heavy snow on Dec. 16	Renhua County
1931	Snow on Dec. 13	Qingyuan City
1932	Cold for several days in Feb.	Xinhui District in Jiangmen City
1933	Snow and the lowest temperature was 0.8 ℃ on Jan. 15	Guangzhou City
1934	Heavy snow in Nov.	Beiliu City
1934	Exremely cold and crops were damaged	Yangshan County
1934	Cold and the lowest temperature was -0.3℃	Guangzhou City
1936	Heavy frost and snow from Dec.17 to Dec. 19	Zijin County
1940	Temperatue was 6.1℃ on Feb. 2	Hong Kong
1941	Extremely cold on Jan. 30 and temperature bleow 4℃ on Feb. 15	Guangzhou City
1942	Heavy snow from Feb. 12 and Feb. 13	Heping County
1943	Snow in early Spring and temperature was -7℃ on Jan. 9	Lechang City
1947	Snow and temperature was 3.1 ℃ Cold wave in late Mar.	Guangzhou City
1949	Dawu mountain snow in late Jan.	Hong Kong